Langtaosha (LTS) Preprint doi: https://doi.org/10.65215/LTSpreprints.2026.11.21.000397. This version posted November 21, 2026. The copyright holder for this preprint (which was not certified by peer review) is the author/funder. Creative Commons license: CC Attribution-NonCommercial-NoDerivatives 4.0 https://creativecommons.org/licenses/by-nc-nd/4.0

A single-cell atlas of *Anopheles stephensi* midgut during *Plasmodium* infection

Abbreviated title: A single-cell atlas of *Anopheles* midgut during *Plasmodium* infection

Authors: Shan Li[1,2§], Guanzhen Fan[2,3§], Wenxu Yang[4], Simin Liang[2], Stephen T. Ferguson[2], Ming Li[5], Zhiyue Lv[5], Jingwen Wang[4*], Feng Liu[2,6*]

1. School of Grain and Food & Pharmacy, Jiangsu Vocational College of Finance & Economics, Huai'an, 223003, China
2. Institute of Infectious Diseases, Shenzhen Bay Laboratory, Shenzhen, 518107, China
3. School of Pharmaceutical Science and Technology, Tianjin University, Tianjin, 300072, China
4. The State Key Laboratory of Genetic Engineering, School of Life Sciences, Fudan University, Shanghai, 200090, China
5. Department of Parasitology, Zhongshan School of Medicine, Sun Yat-sen University, Guangzhou, 510080, China
6. Guangdong Provincial Key Laboratory of Infection Immunity and Inflammation, Shenzhen, China

[*]Corresponding authors: Feng Liu (liufeng@szbl.ac.cn), Jingwen Wang (jingwenwang@fudan.edu.cn)

[§]SL and GF share the first authorship of this article

Langtaosha (LTS) Preprint doi: https://doi.org/10.65215/LTSpreprints.2026.11.21.000397. This version posted November 21, 2026. The copyright holder for this preprint (which was not certified by peer review) is the author/funder. Creative Commons license: CC Attribution-NonCommercial-NoDerivatives 4.0 https://creativecommons.org/licenses/by-nc-nd/4.0

Abstract

As a major vector for malaria, *Anopheles stephensi* poses a considerable threat to countries in South Asia, the Middle East, and Africa, as its expanding range has facilitated the spread of malaria. During infection, *Plasmodium* gametocytes ingested with the blood meal first differentiate into gametes, which undergo fertilization to form zygotes; the zygotes then differentiate into motile ookinetes that traverse the mosquito midgut epithelium approximately 24 hours post-blood meal and subsequently give rise to sporozoites. In this study, we collected midgut tissues from *Anopheles* mosquitoes 24 hours after they fed either a regular or a *Plasmodium*-infected blood meal. Utilizing single-cell RNA sequencing, we comprehensively characterized the changes in cellular composition and transcriptional profiles in midgut cells of *An. stephensi* in response to uninfected blood or *Plasmodium*-infected blood, with the sugar meal serving as a control. We identified major cell types, including intestinal stem cells/enteroblasts (ISCs/EBs), enteroendocrine cells (EEs), enterocytes (ECs), and cardia cells (CAs), using gene markers consistent with those reported in mosquito and *Drosophila* midguts. Our findings revealed that both blood feeding and *Plasmodium* infection alter the cellular composition and transcriptional landscape of the *Anopheles* midgut, particularly through the differential expression of immune-related genes. Notably, we uncovered close interactions between *Plasmodium* ookinetes and multiple types of midgut cells during parasite traversal of the epithelium, suggesting a broad cellular tropism of parasite-vector interactions. Despite the absence of biological replicates and functional validations, this study provides critical single-cell-level insights into how blood feeding and *Plasmodium* infection reshape the cellular composition and transcriptional profile of the mosquito midgut, advancing our understanding of intestinal responses that underpin vector competence.

Keywords: *Anopheles stephensi*, single cell sequencing, midgut, *Plasmodium berghei,* immune genes

Background

Anopheles stephensi, a primary vector of human malaria caused by *Plasmodium* parasites, poses a growing public health threat across South Asia, the Middle East, and eastern Africa, with its range continuing to expand into new regions of the continent [1-3]. Following a blood meal from an infected host, *Plasmodium* gametocytes are ingested into the mosquito midgut lumen. Within this environment, gametogenesis is rapidly induced, leading to the formation of male and female gametes. Fertilization then gives rise to a diploid zygote that differentiates into a motile ookinete. Within approximately 24 hours post-blood meal, the ookinete traverses the midgut epithelial layer–a process that often induces epithelial cell apoptosis or extrusion–before exiting into the hemocoel, where it anchors beneath the basal lamina and develops into an oocyst. During sporogony, each oocyst undergoes extensive asexual replication, producing numerous sporozoites. Upon maturation, the oocyst ruptures, releasing sporozoites into the mosquito hemolymph. These sporozoites then actively migrate to and invade the salivary glands, where they accumulate in the acinar regions. During a subsequent blood meal, sporozoites are

Langtaosha (LTS) Preprint doi: https://doi.org/10.65215/LTSpreprints.2026.11.21.000397. This version posted November 21, 2026. The copyright holder for this preprint (which was not certified by peer review) is the author/funder. Creative Commons license: CC Attribution-NonCommercial-NoDerivatives 4.0 https://creativecommons.org/licenses/by-nc-nd/4.0

expelled along with mosquito saliva into the dermis of a new vertebrate host, thereby initiating hepatic infection [4-6].

The mosquito midgut is a vital organ for food digestion, nutrient absorption, and pathogen entry [7]. Functionally, it is divided into two major regions: the anterior midgut (AMG) and the posterior midgut (PMG). The AMG is primarily responsible for the absorption of sugars, ions, and water, while the PMG is involved in blood digestion [8]. The midgut epithelium is composed of four main cell types: intestinal stem cells (ISC), enteroblasts (EB), enterocytes (EC), and enteroendocrine cells (EE), each defined by their distinct roles. ISCs are undifferentiated adult midgut progenitors distributed throughout the midgut epithelium, capable of differentiating into EEs and ECs to replenish lost cells [9]. EBs represent an intermediate cell state in the differentiation trajectory from ISCs to ECs and EEs, serving as a critical transitional population during midgut epithelial renewal. ECs are the predominant cells in the mosquito midgut, responsible for producing digestive enzymes and absorbing nutrients [10]. Although EEs comprise a small fraction of the total epithelial population, they are vital modulators of homeostasis that synthesize and secrete enteroendocrine peptides in response to various luminal stimuli [11,12]. These peptides regulate physiological processes, including feeding behavior, metabolism, signal transduction, and immunity. Notably, due to anatomical continuity, a small population of cardia cells (CAs) residing at the AMG entrance [13], is frequently identified in studies of midgut cellular heterogeneity [14].

Single-cell RNA sequencing (scRNA-seq) has revolutionized transcriptional analysis by enabling gene expression profiling at single-cell resolution, facilitating detailed investigations into the cellular heterogeneity of the insect midgut and the complex interactions between midgut cells and dietary components (e.g., blood meal), microbiota, and pathogens (e.g., viruses, parasites). For instance, in *Drosophila melanogaster*, integrating single-cell sequencing with a collection of peptide hormone and receptor knock-in strains enabled a comprehensive analysis of the cellular diversity, spatial distribution, and transcription factor code of EEs in the adult midgut [15]. Subsequently, the first full cell atlas of the fly midgut generated using scRNA-seq identified 22 distinct cellular clusters representing ISCs, EBs, EEs, and ECs. This work not only recapitulated known ISC/EB and EE markers but also yielded new insights into intestinal physiology and previously uncharacterized cellular functions [16]. In the context of mosquitoes, scRNA-seq was first employed to characterize hemocytes, confirming the existence of two previously described cell types and uncovering active molecular exchange between them [17], thereby establishing a foundation for the application of single-cell approaches in other mosquito tissues. Subsequently, Cui and co-workers employed single-nucleus RNA sequencing (snRNA-seq) to characterize cellular heterogeneity in the *Aedes aegypti* midgut, delineating the differential transcriptional responses of various cell types to a blood meal. Their study revealed that blood ingestion dramatically alters both the overall cellular composition and transcriptional profiles of the midgut[18].

Langtaosha (LTS) Preprint doi: https://doi.org/10.65215/LTSpreprints.2026.11.21.000397. This version posted November 21, 2026. The copyright holder for this preprint (which was not certified by peer review) is the author/funder. Creative Commons license: CC Attribution-NonCommercial-NoDerivatives 4.0 https://creativecommons.org/licenses/by-nc-nd/4.0

In response to pathogen infection, mosquito midgut epithelial cells activate intrinsic immune signaling pathways and secrete signaling molecules that propagate intercellular and systemic responses, leading to widespread changes in cell composition and transcriptional states. Furthermore, scRNA-seq has also been instrumental in uncovering how distinct cell types differentially reprogram their transcriptomes during infection. For instance, Chen et al. leveraged scRNA-seq data from the *Ae. aegypti* midgut, simultaneously aligning reads to both the *Ae. aegypti* and *Zika* virus reference genomes. This approach allowed them to unambiguously identify virus-positive host cells at single-cell resolution, demonstrating that specific cell types, such as ECs and EEs, are the primary targets of *Zika* virus [19]. In *Culex* mosquitoes, Fitzmeyer et al. used scRNA-seq to construct a single-cell atlas of the *Culex tarsalis* midgut during *West Nile* virus (WNV) infection, revealing significant modulation of midgut cellular composition and gene transcription, particularly of antiviral immune genes [20]. In *Anopheles* mosquitoes, scRNA-seq has unveiled key processes governing parasite developmental transitions and vector-parasite interactions in the midgut of *Anopheles gambiae*, highlighting the specialized roles of different midgut cell types in immune defense, tissue repair, and metabolic adaptation [21].

As a critical barrier against malaria infection, the *Anopheles* mosquito midgut is subject to enormous physiological stress during blood feeding and *Plasmodium* infection [23-25]. This stress intensifies during the traversal of parasite ookinetes 24 hours post-blood meal, a critical phase that we hypothesize triggers marked adaptive responses in terms of cellular composition and transcriptional regulation. Therefore, this study aimed to investigate the cellular composition and transcriptional profiles of midgut cells in *An. stephensi* in response to uninfected and Plasmodium-infected blood meals at single-cell resolution. Despite the absence of biological replicates and functional validations in this exploratory study, our findings provide valuable insights into mosquito intestinal physiology and vector biology, which may facilitate the development of novel strategies for malaria control.

Methods

Mosquito rearing

An. stephensi was used in this experiment. Adult females 3-5 days post-eclosion were selected for uninfected or *Plasmodium*-infected blood-feeding. Mosquitoes were reared in an insectary, kept at 28°C, 80% relative humidity, and maintained under a 12 h light/12 h dark cycle. During the rearing period, a 10% sucrose solution and distilled water were continuously provided to mosquitoes as the basic energy sources during the non-blood-feeding stage.

P. berghei infection

BALB/c mice (Jiesijie Laboratory Animal Co., Ltd, Shanghai, China) were used to provide blood meals for mosquitoes. Specifically, mice in the experimental group were infected with *P. berghei*, and mosquitoes were fed on these infected mice with 3% parasitemia. Following the blood meal, mosquitoes with full abdominal engorgement

Langtaosha (LTS) Preprint doi: https://doi.org/10.65215/LTSpreprints.2026.11.21.000397. This version posted November 21, 2026. The copyright holder for this preprint (which was not certified by peer review) is the author/funder. Creative Commons license: CC Attribution-NonCommercial-NoDerivatives 4.0 https://creativecommons.org/licenses/by-nc-nd/4.0

were selected for subsequent dissection experiments and maintained at 21°C post-feeding. A subset of the selected mosquitoes was dissected to collect their midguts at 24 hours post-infection or after uninfected blood feeding and sugar feeding for single-cell RNA sequencing (scRNA-seq), while the remaining mosquitoes were subjected to oocyst counting at 14 days post-blood meal.

Isolation of *Anopheles* mosquito midguts

Following immobilization of mosquitoes by chilling on ice, dissection was completed as soon as possible within 1 hour. The surfaces of the *Anopheles* mosquitoes were sequentially washed twice with alcohol and phosphate-buffered saline (PBS). Thereafter, the midguts were carefully retrieved and transferred into tissue preservation solution for subsequent single-cell isolation. Each sample was constructed from a total of 400 midguts.

Preparation of single-cell suspensions

Fresh tissues were stored on ice in the sCelLive™ Tissue Preservation Solution (Singleron) within 30 min after dissection. Hanks' Balanced Salt Solution (HBSS) was used three times to wash the specimens, mince them into small pieces, and digest them in 3 mL sCelLiv™ Tissue Dissociation Solution (Singleron) using the Singleron Pytho™ Tissue Dissociation System at 37°C for 15 min. A 40-micron sterile strainer was used to collect and filter the cell suspension. After adding the GEXSCOPE® red blood cell lysis buffer (RCLB, Singleron), the mixture [Cell: RCLB = 1:2 (volume ratio)] was incubated for 5-8 min at room temperature to remove red blood cells. After centrifugation at 300 g 4°C for 5 min, the mixture was gently resuspended in PBS. Finally, Trypan Blue staining was applied to the samples, and cell viability was assessed microscopically.

RT & amplification & library construction

Single-cell suspensions (2×10^5 cells/mL) with PBS (HyClone) were placed onto a microwell chip using the Singleron Matrix® Single Cell Processing System. Reverse transcription of the mRNA captured by the Barcoding Beads was followed by PCR amplification of the cDNA generated from the Barcoding Bead collection. Sequencing adapters were then ligated to the fragmented cDNA. GEXSCOPE® Single Cell RNA Library Kits (Singleron) were used to construct the scRNA-seq libraries. Illumina NovaSeq 6000 was used to sequence 150-bp paired-end reads from individual libraries diluted to 4 nM, pooled, and processed. qPCR was performed with Illumina adapter-specific primers to quantify library concentration and ensure valid amplification.

Primary analysis of raw read data

Gene expression matrices were generated using CeleScope (https://github.com/singleron-RD/CeleScope) v1.9.0 pipeline from raw scRNA-seq reads. Raw reads were first processed with CeleScope to remove low-quality reads by applying default parameters (e.g., limitBAMsortRAM=32, 000, 000, 000, outFilterMatchNmin=30, outSAMtype=BAM, skip_read=10,000, use_read=1,000). Next, cell barcodes and UMI

Langtaosha (LTS) Preprint doi: https://doi.org/10.65215/LTSpreprints.2026.11.21.000397. This version posted November 21, 2026. The copyright holder for this preprint (which was not certified by peer review) is the author/funder. Creative Commons license: CC Attribution-NonCommercial-NoDerivatives 4.0 https://creativecommons.org/licenses/by-nc-nd/4.0

(Unique Molecular Identifiers) were extracted. Next, we mapped reads to the reference genome *An. stephensi* UCISS2018 (VectorBase version 68 annotation) using STAR v2.6.1a [25]. Finally, each cell's UMIs and gene counts were acquired with featureCounts v2.0.1 [26] software and used to generate expression matrix files for subsequent analysis.

Quality control, dimension reduction, and clustering

Seurat 5.5.1 [27] in R v4.5.2 was used to perform quality control, dimension reduction, and clustering. The expression matrix for each sample dataset was filtered by the following criteria: 1) genes expressed in fewer than 5 cells were excluded; 2) ambient RNA contamination was mitigated using decontX v1.8.0; 3) doublet identification was performed with DoubletFinder (v2.0.6); 4) cells with a gene count of less than 200 were excluded; 5) cells with a UMI count of less than 200 or more than 5000 were excluded; 6) cells with mitochondrial gene content >20% were excluded. After filtering out the doublets, all 3 samples were normalized using the NormalizeData function, scaled using ScaleData (regressing out the percentage of mitochondrial gene content), and integrated using IntegrateLayers with the HarmonyIntegration method. The top 2000 variable genes were selected. Principal Component Analysis (PCA) was performed on the scaled variable gene matrix, and the top 17 principal components were used to reduce the dimensions and cluster the cells. Cells were split into clusters using the Louvain algorithm with a resolution parameter of 0.7. Cell clusters were visualized using Uniform Manifold Approximation and Projection (UMAP). To ensure full reproducibility and allow for public evaluation, the complete analysis scripts and code are available in a public GitHub repository (https://github.com/Junetea/Anopheles_midgut_scRNA).

Trajectory analysis

UMAP-based Monocle 3 was adopted to infer the developmental trajectory of the midgut [28]. CAs were excluded before the analysis was performed. ISC/EBs were specified as the starting point.

Differentially expressed gene (DEG) analysis

To identify differentially expressed genes (DEGs), we used the Seurat FindMarkers function based on the Wilcoxon rank-sum test with default parameters. We selected the genes expressed in more than 10% of the cells in a cluster, with an average log fold-change value greater than 0.25 as DEGs. The cell types of each cluster were annotated using the DEGs and knowledge from the literature regarding canonical markers. The expression of markers in each cell type was displayed using heatmaps/dot plots/violin plots generated with the Seurat DoHeatmap/DotPlot/Vlnplot functions. Homology searches using the BLAST (v2.5.0+) program against the protein sequences in the database of insect immune-related proteins (ImmunoDB) [29] with an E-value cutoff $1e^{-5}$, which allowed us to identify orthologous genes in *An. stephensi*.

Cell type annotation

Existing marker genes of *Drosophila*, *Ae. aegypti*, and *An. gambiae* midguts were used to identify the cell types. In addition, Seurat was used to generate heatmaps/dot plots/violin

Langtaosha (LTS) Preprint doi: https://doi.org/10.65215/LTSpreprints.2026.11.21.000397. This version posted November 21, 2026. The copyright holder for this preprint (which was not certified by peer review) is the author/funder. Creative Commons license: CC Attribution-NonCommercial-NoDerivatives 4.0 https://creativecommons.org/licenses/by-nc-nd/4.0

plots that illustrated the expression of markers.

Pathway enrichment analysis

TBtools-II was used to analyze Gene Ontology (GO) and Kyoto Encyclopedia of Genes and Genomes (KEGG) data to investigate DEG functions [30]. Pathways with an adjusted p value less than 0.05 were considered significantly enriched. Gene Ontology gene sets, including molecular function (MF), biological process (BP), and cellular component (CC) categories, were used as references.

scRNA-seq-based *Plasmodium* detection.

The same reads, mapped to the *P. berghei* genome obtained from the National Center for Biotechnology Information (NCBI), were used as part of the comprehensive analysis. CeleScope pipeline was used to generate the matrix data, which were quality-controlled using the same Seurat pipeline and filtering criteria as applied to the midgut cells. Integration of *An. stephensi* and *P. berghei* single-cell data via shared barcodes was used to identify the infected midgut cells during malaria parasite invasion. Midgut cells whose barcodes matched with those of at least one *Plasmodium* cell were therefore defined as infected cells.

Results

Moderate infection level of *An. stephensi* by *Plasmodium berghei*

To investigate the cellular and transcriptional responses of the mosquito midgut to the traversal of motile ookinetes of *P. berghei*, we collected midgut tissue samples 24 hours after an infected blood meal (Fig. 1A). To verify infection intensity, a subset of the infected *An. stephensi* were reared until day 14 post-infection, at which point they were sacrificed for midgut dissection. As expected, most midguts harbored *Plasmodium* oocysts with a median intensity of three oocysts per midgut (Fig. 1B). This closely mirrors natural infection intensities observed in the field, such as in West Africa, where the majority of wild-caught infected mosquitoes carry no more than five oocysts per midgut [31]. Among the 20 midguts examined, 16 contained *Plasmodium* oocysts, yielding an infection prevalence of 80%. Therefore, this moderate *P. berghei* infection level likely represents the genuine physiological challenge experienced by mosquitoes in nature, rather than the artificially intense laboratory infection characterized by dozens or hundreds of oocysts per midgut [33-35].

Single-cell RNA sequencing and cell type identification in the mosquito midgut

scRNA-seq was performed on pools of *An. stephensi* midguts 24 hours post-feeding with either a *Plasmodium*-infected blood meal or an uninfected blood meal. As a control, midgut samples from mosquitoes fed a regular sugar solution (10% sucrose) were included. The specific sequencing statistics for each sample, including the total number of reads, the total number of cells, and the median number of genes and UMIs detected per cell, can be found in Table S1. The resulting single-cell transcriptomes captured 96.4% of the 14,966 annotated genes in the *An. stephensi* genome. Following the removal of low-quality cells and putative doublets, 5,349 (sugar-fed), 7,236 (blood-fed), and

Langtaosha (LTS) Preprint doi: https://doi.org/10.65215/LTSpreprints.2026.11.21.000397. This version posted November 21, 2026. The copyright holder for this preprint (which was not certified by peer review) is the author/funder. Creative Commons license: CC Attribution-NonCommercial-NoDerivatives 4.0 https://creativecommons.org/licenses/by-nc-nd/4.0

7,946 (*Plasmodium*-infected) cells were retained for downstream analysis (Table S2; Fig. S1-2).

To investigate the effects of blood feeding and *P. berghei* infection on gene expression and cellular composition in the *An. stephensi* midgut, distinct cell clusters were identified from the integrated data of all three conditions using Seurat and visualized via UMAP. Cluster identities were assigned based on previously established gene markers for specific cell types in *Drosophila* [16] and *Ae. aegypti* midguts [14], as well as statistically identified marker genes (Fig. 2A). As expected, all major midgut cell types were successfully annotated, including ISC/EB, EC-like_1, EC-like_2, EC, EE, and CA (Table 1; Fig. 2B). Pseudotime trajectory analysis of the epithelial cell clusters (ISC/EB, EE, EC, EC-like_1, and EC-like_2) revealed three distinct developmental lineages: ISC/EB to EE, ISC/EB to EC/EC-like_1, and ISC/EB to EC/EC-like_2, which aligns well with existing biological paradigms [9,16,35](Fig. S3).

Clustering of individual midgut samples revealed distinct cellular compositions among mosquitoes under different feeding conditions. Notably, a substantial difference in the proportion of enterocytes (EC-likes) was observed between sugar-fed and blood-fed mosquitoes. The EC-like_1 cluster was considerably enriched in both infected and uninfected blood-fed mosquitoes compared to sugar-fed controls, whereas the EC-like_2 cluster was predominantly detected in sugar-fed mosquitoes and was nearly absent in blood-fed ones (Fig. 2C-E), suggesting a substantial remodeling of midgut cellular composition in response to blood feeding. Specifically, the ISCs/EBs cluster was characterized by the high expression of marker genes, including *Tk* (*Tachykinin*, ASTEI20_033599), *Delta* (ASTEI20_036824), *Klu* (*Klumpfuss*, ASTEI20_041957), and *E(spl)m3-HLH* (ASTEI20_039126) (Fig. 2A, D, E). The EE cluster was defined by the significant expression of *Pros* (*Prospero*, ASTEI20_044963) and/or *NFP* (ASTEI20_040636), as well as *Dh31* (ASTEI20_032396) and *CCha2* (ASTEI20_036596) (Fig. 2A, H). The cardia cell (CA) cluster was identified by the strong expression of *CTL* (*C-type lysozyme*, ASTEI20_039435), *Tret1* (ASTEI20_039362), and *Gambicin* (ASTEI20_032045) (Fig. 2A, I). Furthermore, EC-like_1 cells exhibited high expression of *trypsin-1* (ASTEI20_041338) and *trypsin-7* (ASTEI20_034155) (Fig. 2A, K), while the EC-like_2 cluster showed robust expression of genes involved in water and ion absorption, including *trypsin-5* (ASTEI20_042351), *CAH2* (ASTEI20_033917), *AQPcic* (aquaporin, ASTEI20_032608), *AQPAn.G* (ASTEI20_042302), and *Nha1* (ASTEI20_039638) (Fig. 2A, F). Although previous studies have reported that *nubbin* (ASTEI20_034725) is highly expressed in the ECs of both *Ae. aegypti* and *D. malenogaster* [14,16], we observed strong *nubbin* expression in only a small fraction of ECs in *An. stephensi* (Fig. 2A, J), suggesting a species-specific expression pattern.

After defining the major cell types of the midgut epithelium, we further explored functionally distinct subpopulations by performing subclustering at a higher resolution (Fig. 3). Our analysis revealed 19 distinct cell subtypes. Notably, the gene *Klu* was highly expressed in a subset of ISC/EBs, particularly in the subclusters ISC/EB-4 and ISC/EB-5.

Langtaosha (LTS) Preprint doi: https://doi.org/10.65215/LTSpreprints.2026.11.21.000397. This version posted November 21, 2026. The copyright holder for this preprint (which was not certified by peer review) is the author/funder. Creative Commons license: CC Attribution-NonCommercial-NoDerivatives 4.0 https://creativecommons.org/licenses/by-nc-nd/4.0

The EE cell type could be further subdivided into three subclusters: EE-1 was characterized by high expression of *Pros, NPF*, *Tachykinin*, and *Dh31*; EE-2 selectively expressed *Pros, NPF* and *CCHa2* whereas EE-3 uniquely expressed *Pros* and *Orco* (*orcokinin*, ASTEI20_032590) along with *tachykinin* but lacked *NPF* and *CCHa2*. Among the two subclasses of Cardia cells marked by *Gambicin* and *Tret1*, subset CA-1 exhibited elevated expression of *CTL*. Detailed analysis of five EC-like_1 subclusters revealed that although EC-like_1-1 to EC-like_1-5 expressed high levels of digestive enzymes, most notably trypsin-related proteases, EC-like_1-4 was uniquely characterized by the expression of enzymes involved in lipid digestion, such as *lipase-H* (ASTEI20_035847). This suggests that specific EC-like_1 subsets may be functionally specialized for processing different dietary components. Finally, further analysis of the EC-like_2 cluster revealed that these cells can be subdivided into two major groups with distinct marker gene expression patterns. For example, EC-like_2-1 and EC-like_2-2 highly expressed *AQPcic,* which is involved in water absorption, while EC-like_2-3 showed strong expression of a *cp-like* gene (carboxypeptidase-like, ASTEI20_041502) that may be involved in protein digestion [36](Fig. 2A, Fig. 3).

Bloodmeal ingestion modulates the cell composition of the mosquito midgut

Blood feeding provides critical nutrients for egg development in female mosquitoes while simultaneously imposing significant physiological stress on the midgut structure and transcriptome during digestion[37,38]. To investigate the impact of blood feeding on the cellular composition of the midgut epithelium, we systematically examined shifts in cell type proportions in *Anopheles* mosquitoes following sugar or blood feeding. Pronounced differences in midgut cellular composition were observed between sugar-fed and blood-fed mosquitoes, characterized by increased numbers of EC, CA, EC-like_1, and EE cells in blood-fed *An. stephensi*, accompanied by a decline in ISC/EB abundance. Specifically, EC-like_1 cells expanded from 1.33% to 48.12%, CAs increased from 17.72% to 19.73%, and EEs rose from 2.79% to 3.94%, while ISC/EBs declined from 37.18% to 25.48% (Table 1). Notably, EC-like_2 cells were detected exclusively in sugar-fed mosquitoes, accounting for 39.82% of the population, whereas the EC-like_1 population was more abundant after uninfected and *Plasmodium*-infected blood-feeding (Fig. 2D, E). These findings align with previous studies on blood-induced cell proliferation in the mosquito midgut, particularly regarding the EC cells in *An. gambiae* [9].

Heterogeneity was also observed in the population dynamics among subclusters of different cell types. For instance, following blood feeding, ISC/EB-1 and ISC/EB-2 increased in abundance, whereas ISC/EB-3, ISC/EB-4, and ISC/EB-5 exhibited an decreased proportion. All five EC-like_1 subclusters increased in abundance after blood feeding. Notably, EC-like_1-1, EC-like_1-2, and EC-like_1-3, which were nearly undetectable in sugar-fed mosquitoes, appeared to be exclusively induced by blood feeding. Regarding the CA cell cluster, the relative proportion of CA-1 cells increased after blood feeding. Conversely, the CA-2 subcluster exhibited a decrease in relative proportion following blood feeding. Additionally, all three EE subclusters (EE-1, EE-2,

Langtaosha (LTS) Preprint doi: https://doi.org/10.65215/LTSpreprints.2026.11.21.000397. This version posted November 21, 2026. The copyright holder for this preprint (which was not certified by peer review) is the author/funder. Creative Commons license: CC Attribution-NonCommercial-NoDerivatives 4.0 https://creativecommons.org/licenses/by-nc-nd/4.0

and EE-3) increased slightly in abundance after blood feeding, rising from 0.92%, 0.65%, and 1.22% to 1.27%, 0.72%, and 1.95%, respectively (Table 2).

Blood meal affects the transcriptional profiles of the mosquito midgut

Numerous bulk RNA-seq studies have demonstrated extensive transcriptional regulation in the mosquito midgut induced by blood feeding [39-41]. To assess the impact of blood feeding on the transcriptional profiles across diverse midgut cell types, we conducted a comprehensive comparison of transcript abundance between sugar-fed and uninfected blood-fed mosquitoes. Using FindMarkers, we identified 378 upregulated and 121 downregulated genes in blood-fed mosquitoes compared to sugar-fed controls (fold change ≥ 2, adjusted p value < 0.05; Table S3). GO enrichment analysis of genes upregulated in response to blood feeding revealed significant enrichment in enzyme activity, protein metabolism, organic acid metabolism, and fatty acid metabolism (Fig. 4A), highlighting the metabolic reprogramming of midgut cells following blood meal ingestion. For instance, blood-fed mosquitoes initiated the expression of metabolic enzymes specifically associated with blood nutrient digestion, including protein-digesting chymotrypsin (*CHYMO*, ASTEI20_034096), three fatty acid-metabolizing hydroxylases (*FAAH2* (ASTEI20_033374), *FAH2* (ASTEI20_034108, ASTEI20_043938)), and a triglyceride-hydrolyzing lipase (ASTEI20_044825) (Fig. 4B). Additionally, several genes involved in transcription and cellular architecture were upregulated, such as *aladin* (ASTEI20_031384) and DNA replication licensing factors *MCM4* (ASTEI20_032850) and *MCM7* (ASTEI20_036152), suggesting a transition toward enhanced metabolic and structural activity in response to blood feeding (Fig. 4B).

Distinct cell types exhibited divergent transcriptional regulation. Both EC-like_1 and EC-like_2 clusters expressed high levels of certain trypsin-like genes. However, the specific trypsin-like gene expressed in *An. stephensi* midgut differed markedly between sugar-fed and blood-fed conditions: *Trypsin-1* and *trypsin-7* were highly expressed in the EC-like_1 cluster of blood-fed mosquitoes, whereas *trypsin-5* was expressed in EC-like_2 cluster of sugar-fed mosquitoes (Fig. 3). Comparative analysis of differentially expressed genes between the EC-like_1 and EC-like_2 clusters revealed that EC-like_2 cells predominantly expressed genes such as carbonic anhydrase (*CAH2*, ASTEI20_033917), glucose dehydrogenase (*GLD*, ASTEI20_045421), aquaporins (ASTEI20_032608), and sodium ion exchangers (*NHA9B2*, ASTEI20_039638), which are implicated in carbohydrate metabolism (Fig. 4C). In contrast, the EC-like_1 cluster showed higher expression of enzymes associated with blood digestion, such as collagenases and carboxypeptidases, as well as genes involved in signal transduction, including neutral ceramidase (Table S4). Additionally, several immune-related genes were also enriched in this cluster, such as CLIP-related protein (ASTEI20_034003), and cell death abnormality protein 1 (ASTEI20_034270) (Table S4). These findings align with previous studies indicating that blood feeding induces robust immune responses in both *Aedes* and *Anopheles* mosquitoes [43-45].

In EE cells, the expression of canonical marker genes, including *Pros*, *NPF*, and *Orco*,

Langtaosha (LTS) Preprint doi: https://doi.org/10.65215/LTSpreprints.2026.11.21.000397. This version posted November 21, 2026. The copyright holder for this preprint (which was not certified by peer review) is the author/funder. Creative Commons license: CC Attribution-NonCommercial-NoDerivatives 4.0 https://creativecommons.org/licenses/by-nc-nd/4.0

remained largely stable between sugar-fed and blood-fed *Anopheles* midguts (Fig. 3). Interestingly, blood feeding caused a significant upregulation of genes involved in innate immunity and cellular homeostasis in EE cells after blood feeding (adjusted p-value < 0.05), such as three Niemann-Pick type C2 (*NPC2*) genes (ASTEI20_031615, ASTEI20_035338, and ASTEI20_039804), which have been previously implicated in antiviral immunity (Fig. 4D, Table S5). In the CA cell cluster, marker genes including *Gambicin*, *Tret1*, and *CTL* were highly expressed in both sugar-fed and blood-fed mosquitoes. Nevertheless, heterogeneity was observed among subpopulations. Specifically, *Gambicin* expression in CA-2 was upregulated after blood feeding, whereas CA-1 displayed reduced expression of *Tret1* and *CTL* with no significant change in *Gambicin* (Fig. 3). Furthermore, we observed a broad and coordinated upregulation of immune effector genes in CA cells following blood feeding, including serine proteases, *NPC2* genes, and key antimicrobial peptides such as cecropin and defensin, suggesting robust activation of the mosquito immune system in response to blood feeding (Table S6).

Plasmodium **detected at varying levels in all cell types of the mosquito midgut**

The traversal process of *Plasmodium* parasites through the midgut epithelium involves close interactions with diverse cell types of the mosquito midgut [21, 45]. To investigate specific midgut cell types interacting with these parasites, we focused on “dual-read” cells capturing transcripts from both *P. berghei* and *An. stephensi*. In midgut cells from mosquitoes fed on a *Plasmodium*-infected blood meal, we detected a total of 607 microwells containing *Plasmodium* reads. After quality control, 43 of these were coexisting with mosquito cells, which we defined as cells with dual-read host-parasite barcodes. Surprisingly, we found that these dual-read cells were broadly distributed across all cell types of the mosquito midgut epithelium, except for EC-like cells, which were only detected in the midgut of sugar-fed mosquitoes. Specifically, among the 43 *Plasmodium*-infected midgut cells, 17, 7, 17, and 2 belonged to ISC/EB, EE, EC-like_1, and CA cells, respectively (Fig. 5A). Analysis of the proportion of different cells with dual-read host-parasite barcodes further revealed that ISC/EB (0.63%) and EE (0.69%) showed the highest *Plasmodium* infection rates; EC-like_1 (0.53%) cells displayed intermediate infection, while CA (0.21%) cells were least likely to be infected (Fig. 5B), suggesting a cell type-dependent bias of parasite infection in the mosquito midgut.

Plasmodium **infection affects the cellular heterogeneity of the mosquito midgut**

To uncover *Plasmodium*-induced alterations in midgut cellular heterogeneity, we compared the proportional distribution of distinct midgut cell types between *Anopheles* mosquitoes fed on *Plasmodium*-infected blood and those fed on uninfected blood, which revealed substantial remodeling of midgut cell composition. Specifically, the proportions of EC cells, EC-like_1s, and CA cells were 1.04%, 40.33%, and 11.98%, respectively, which were lower than those in the uninfected group. In contrast, the proportions of EE cells and ISC/EB cells were higher than those in the uninfected group (12.76% versus 3.94%, 33.88% versus 25.48%, respectively) (Table 1), which aligns with recent work showing a *Plasmodium*-induced increase of approximately 4% in *Anopheles* midgut

Langtaosha (LTS) Preprint doi: https://doi.org/10.65215/LTSpreprints.2026.11.21.000397. This version posted November 21, 2026. The copyright holder for this preprint (which was not certified by peer review) is the author/funder. Creative Commons license: CC Attribution-NonCommercial-NoDerivatives 4.0 https://creativecommons.org/licenses/by-nc-nd/4.0

progenitor cells at one day post-blood-feeding, as quantified by fluorescence staining [45].

Detailed analysis of subtypes within the same cell cluster revealed heterogeneous population dynamics in response to *Plasmodium* infection (Table 2). We observed that the proportions of all three EE subclusters were higher in mosquitoes fed on *Plasmodium*-infected blood meals than those fed on uninfected blood meals. Among the five ISC/EB subclusters, subclusters ISC/EB-2, -3, -4, and -5 were more abundant in the infected blood-fed sample, whereas subcluster ISC/EB-1 exhibited almost the same proportion with no drastic change. In addition, the proportions of both CA subtypes (CA-1 and CA-2) were lower in the infected blood-fed sample than those in the uninfected blood-fed sample. Within the EC subtypes, we observed divergent trends: some subtypes accounted for a larger proportion of cells in the infected blood-fed sample, while others showed a smaller proportion. Subclusters EC-like_1-2, -3, and -4 exhibited increased proportions after blood feeding, and this expansion was enhanced upon *Plasmodium* infection. In contrast, the proportions of subclusters EC-like_1-1 and -5 were higher in the midgut of uninfected blood-feeding mosquitoes compared with those in the infected blood-feeding mosquitoes.

Plasmodium infection affects the transcript profiles of the mosquito midgut

To further elucidate the effects of *Plasmodium* infection on gene transcript levels in the mosquito midgut, we used FindMarkers to identify 257 protein-coding genes that were significantly up-regulated (fold change ≥ 2, adjusted p value < 0.05) in mosquitoes fed on *Plasmodium*-infected blood compared with those fed on uninfected blood (Table S7). Notably, we found that the heat shock proteins *Hsp70A1* (ASTEI20_036856), *Hsp83* (ASTEI20_041157), *Hsp83-like* (ASTEI20_042101), and *Hsp70A1-like* (ASTEI20_043376) were markedly overexpressed in the midgut of mosquitoes fed on infected blood (Fig. 6A). Heat shock proteins have been previously reported to protect the mosquito midgut from stress [46,47] and may be involve in the defense of *Plasmodium* invasion [48]. Moreover, several cell signaling and proliferation-related genes were also found to be transcriptionally elevated, potentially contributing to the maintenance of internal homeostasis. These include the *diuretic hormone receptor* (*Dh-like*, ASTEI20_044112) and *adenosine deaminase 2* (*ADA2*, ASTEI20_041621) [50, 51] (Fig. 6A).

To gain insight into the pathways underlying *Plasmodium*-triggered transcriptional modulation in the mosquito midgut, we performed KEGG pathway analysis on the upregulated genes and identified two activated pathways following *Plasmodium* exposure: the MAPK and Hippo pathways (Table S8). As indicated in previous studies, the MAPK pathway is important for wound healing and tissue repair, while the Hippo pathway is critical for regulating cell proliferation and tissue homeostasis [50,51]. Both pathways may be actively involved in the defense against parasite invasion in the mosquito midgut [52]. Close examination of the genes involved in these pathways revealed that the *RAS2* gene (*KSR2*, ASTEI20_041433) and lipoma-preferred partner gene (*Zyx*,

Langtaosha (LTS) Preprint doi: https://doi.org/10.65215/LTSpreprints.2026.11.21.000397. This version posted November 21, 2026. The copyright holder for this preprint (which was not certified by peer review) is the author/funder. Creative Commons license: CC Attribution-NonCommercial-NoDerivatives 4.0 https://creativecommons.org/licenses/by-nc-nd/4.0

ASTEI20_040828) were markedly upregulated in the midgut of mosquitoes fed on infected blood compared with those fed on uninfected blood (Table S8). *RAS2* functions as a kinase suppressor in the MAPK pathway[56-58], while Zyx is a known regulator of cell proliferation and viral infection in mosquitoes within the Hippo pathway[56].

We observed that while blood feeding induces dramatic metabolic responses in the midgut , *Plasmodium* infection appears to reprogram this response, leading to metabolic responses distinct from those in uninfected blood-fed mosquitoes. For example, although xenobiotic, amino acid, and lipid metabolism were induced by blood feeding (Fig. 6B), *Plasmodium* infection further activated both nucleotide and terpenoid/polyketide metabolisms, indicating a pathogen-associated metabolic signature in the mosquito midgut (Fig. 6C). Consistent with studies in other insects, these metabolic pathways are implicated in immune regulation, suggesting a potentially conserved role for metabolism in host-pathogen interactions [60-64].

Additionally, a detailed analysis of transcriptional regulation across distinct cell clusters reveals diverse response patterns to parasite infection. GO enrichment analysis of upregulated genes in ECs revealed significant enrichment in biosynthetic activities, signaling, and stress responses (Fig. S4A). Notably, *carbonic anhydrase 7* (CAH7, ASTEI20_032202), which is involved in cell homeostasis, and *adenosine deaminase 2-like* (*ADA2*), which plays a role in antiviral immunity [62], were among the upregulated genes (Fig. S4B). Moreover, we observed that EEs were enriched for Hsp-like genes associated with cellular heat response, including *Hsp70A1, Hsp83*, and *Hsp83-like* (Fig. S5).

Plasmodium infection modulates the expression of immune genes in different cell types of the mosquito midgut

To further investigate the *Plasmodium*-induced immune response in the midgut of *An. stephensi*, immune-related genes that exhibited either high expression levels or broad expression across multiple cell types were selected for detailed examination. We then constructed heatmaps representing the average transcription level of specific immune genes within each cell cluster (Fig. 7), highlighting the differential expression patterns of immune genes across distinct cell populations in the mosquito midgut.

To ensure data reliability, we first assessed the consistency of midgut samples from mosquitoes on different diets by analyzing the expression of the housekeeping gene *RPL19* (ASTEI20_030840). Indeed, *RPL19* was relatively stably expressed across all midgut samples, with a coefficient of variation of 0.353 and the absolute $\log_2$ fold change ($\log_2$FC) ranging from 0.14 to 0.38, suggesting that its expression was relatively consistent across experimental conditions and thus supporting the robustness of our datasets (Fig. S6, Table S9). We then focused on the innate immune system-the primary line of defense against microbial pathogens in mosquitoes. Key immune-related genes from canonical immune pathways, including Toll, JAK-STAT, IMD, RNAi, as well as genes involved in antimicrobial peptide (AMPs) production and apoptosis, were selected

Langtaosha (LTS) Preprint doi: https://doi.org/10.65215/LTSpreprints.2026.11.21.000397. This version posted November 21, 2026. The copyright holder for this preprint (which was not certified by peer review) is the author/funder. Creative Commons license: CC Attribution-NonCommercial-NoDerivatives 4.0 https://creativecommons.org/licenses/by-nc-nd/4.0

for in-depth analysis. These pathways are evolutionarily conserved and known to mediate defense against pathogenic bacteria, fungi, and parasites. By examining their expression patterns across cell clusters, we aimed to compare the transcriptional dynamics of immune genes in the midguts of blood-fed and *Plasmodium*-infected blood-fed *Anopheles* mosquitoes.

The mosquito midgut immune response to *Plasmodium* infection involves several steps, including *Plasmodium* pattern recognition, signal transduction, and signal modulation [63]. Indeed, we identified several pattern recognition receptor (PRR) genes that were upregulated following *Plasmodium* infection across different midgut cell types. These included scavenger receptors (SCRs) such as *SCRB7* (ASTEI20_042413) in the EC cell cluster and *SCRAC1* (ASTEI20_035300) across all cell clusters (Fig. 7). In addition, *GALE3* (ASTEI20_041298), which may facilitate pathogen adhesion to host cells and activate host immunity [65,66], was also found to be upregulated in all cell cluster (Fig. 7).

Several genes associated with the TOLL and IMD pathways were transcriptionally regulated in the *Plasmodium*-infected blood-fed mosquito midgut compared to the uninfected control. For instance, *dorsal* (ASTEI20_044951) and ASTEI20_038199 of the TOLL pathway in EC cells and *akirin* (ASTEI20_043767) of the IMD pathway in both EC and EC-like_1 cells were overexpressed in the infected blood-fed mosquito midgut (Fig. 7). In addition, we found that *Stat92E* (ASTEI20_034602) and *Dome* (ASTEI20_036821) linked to the JAK-STAT pathway [69,70], were up-regulated in EC and EC-like_1 cells. Furthermore, the *Drosha* gene (ASTEI20_040616), which inhibits *P. berghei* infection via the RNAi pathway [71,72], was upregulated in EE and EC-like_1 cells(Fig. 7). Taken together, the coordinated regulation of multiple immune-related genes suggests distinct patterns of signal transduction pathway activation across different cell clusters in response to *Plasmodium* infection. Furthermore, several immune modulators known to enhance signal amplification through protease cascades during pathogen invasion [75-77] were observed to be overexpressed in different cell clusters following a *Plasmodium*-infected blood meal. These included *CLIPB16* (ASTEI20_038438) in the ISC/EB, EC, and EC-like_1 clusters; *CLIPC3* (ASTEI20_045150) in the EC and EC-like_1 clusters; and *CLIP5B* (ASTEI20_030906) in EE cells (Fig. 7).

Discussion

In this study, we identified several canonical cell populations in the midgut of An. stephensi, including ISCs/EBs, EEs, ECs, and CAs, which align with previous studies on the midguts of other haematophagous and non-haematophagous insects, such as Aedes mosquitoes (*Ae. aegypti*), fruit flies (*D. melanogaster*), silkworms (*Bombyx mori*), and fall armyworms (*Spodoptera frugiperda*) [80-83], suggesting conserved cellular organization and functions in nutrient digestion, absorption, and pathogen defense. Nevertheless, we did not detect goblet cells (GCs) in the An. stephensi midgut. GCs are also absent in the midgut of fruit flies and Aedes mosquitoes but appear to exist in some

Langtaosha (LTS) Preprint doi: https://doi.org/10.65215/LTSpreprints.2026.11.21.000397. This version posted November 21, 2026. The copyright holder for this preprint (which was not certified by peer review) is the author/funder. Creative Commons license: CC Attribution-NonCommercial-NoDerivatives 4.0 https://creativecommons.org/licenses/by-nc-nd/4.0

lepidopteran insects [82,83], suggesting a potential functional substitution by other epithelial cell types and evolutionary conservation within the Dipteran. Moreover, despite our exhaustive efforts to identify visceral muscle cells with multiple classical gene markers, including Mlc (myosin light chain), Mhc (myosin heavy chain), and muscle actins [14,35], and by adjusting clustering parameters, we failed to detect or unambiguously define a visceral muscle population in the An. stephensi midgut. Therefore, to avoid potential misinterpretation of our sequencing results, we chose to omit visceral muscle from our cellular annotation. Interestingly, previous cellular profiling studies of the midguts of Ae. aegypti, fruit flies, and fall armyworms also failed to recover visceral muscle cells [16,19,82], suggesting potential technical limitations in pre-sequencing cell filtering/processing before sequencing or in gene annotation algorithm.

Our study further demonstrated that blood meal ingestion induces considerable alterations in both the cellular composition and transcriptional profiles of the *Anopheles* midgut. Notably, we identified a distinct cluster of enterocyte-like (EC-like_2) cells that were exclusively present in sugar-fed mosquitoes but absent in blood-fed counterparts. In contrast, EC-like_1 cells and a subpopulation of ISC/EB cells were detected only in blood-fed *Anopheles* mosquitoes, but not in sugar-fed ones. Additionally, the midgut epithelium undergoes profound physiological transformation following blood feeding, transitioning from a quiescent, sugar-metabolizing state to an active state of digestion and regeneration. This transition is characterized by coordinated upregulation and widespread transcriptional activation of metabolic pathways governing lipid and amino acid processing, reflecting the tissue's adaptive response to nutrient influx. Interestingly, a previous snRNA-seq study led by Cui et al. on the *Ae. aegypti* midgut reported dramatic, blood meal-induced changes in cell type composition, with three specific clusters (EC-like_1-1, -2, and -3) exclusively identified in blood-fed mosquitoes but not in sugar-fed ones [19]. Furthermore, this same study observed upregulation of genes involved in metabolic processes (including organonitrogen compound, carbohydrate, and small molecule metabolism) and ion transport [18]. These findings suggest a conserved shift in midgut cell composition and transcription triggered by the blood meal between *Aedes* and *Anopheles* mosquitoes, whose last common ancestor lived approximately 179 million years ago[84].

scRNA-seq of *Plasmodium*-infected mosquito midguts enabled the identification of potential host-parasite interactions. Parasites captured either within midgut cells or in close association with them would share the same cellular barcode as the host cell, a phenomenon we defined as “dual-read” cells. Our analysis revealed that *P. berghei* exhibits broad infection tropism, with ookinetes invading all major midgut epithelial cell types, particularly ISCs, EEs, and EC-like-1s. Supporting this finding, a recent study by Barletta et al. (2024) using cellular staining/imaging demonstrated that at 24 hours post-infection, approximately 4% of *P. berghei* ookinetes were closely associated with midgut progenitor cells (ISCs/EBs) [45]. This proportion of parasites associated with progenitors increased to 46% by 5 days post-infection (at the oocyst

Langtaosha (LTS) Preprint doi: https://doi.org/10.65215/LTSpreprints.2026.11.21.000397. This version posted November 21, 2026. The copyright holder for this preprint (which was not certified by peer review) is the author/funder. Creative Commons license: CC Attribution-NonCommercial-NoDerivatives 4.0 https://creativecommons.org/licenses/by-nc-nd/4.0

stage), with most oocysts (85%) maintaining direct contact with midgut progenitors at 10 days post-infection, highlighting the extensive interaction between progenitor cells and parasites. Parallel evidence comes from a study investigating *P. falciparum* and *An. gambiae* midgut interactions, which combined scRNA-seq and cell staining/imaging to identify a small population of parasite-infected midgut cells, primarily comprising progenitor cells (ISCs/EBs) and, to a lesser extent, posterior enterocytes (pECs) [22]. These findings collectively demonstrate the efficacy of scRNA-seq in capturing host-parasite cellular interactions and reveal a previously unrecognized bias in *Plasmodium* interactions with midgut progenitor cells during the parasite's traversal of the midgut epithelium prior to oocyst establishment.

In addition, while blood meals are essential for mosquito survival and reproduction, the ingestion of blood introduces mechanical, chemical, and biological stresses. Blood often contains large amounts of cytotoxic molecules, such as haem, and infectious pathogens like mosquito-borne viruses (Dengue and Zika viruses) and parasites (*Plasmodium*). These factors pose huge challenges to the cellular structure and physiology of the mosquito midgut, triggering defense strategies such as increased cell turnover and upregulation of immune-related genes to counteract these abiotic and biotic stresses [22,41,85,86]. Our single-cell analysis further indicated that blood feeding itself induces epithelial damage, triggering DNA repair mechanisms and stimulating stem cell-driven renewal to maintain midgut integrity. *Plasmodium* infection exacerbates this damage by directly causing host cell death, which further amplifies regenerative demand and accelerates epithelial turnover. At the molecular level, we found that *Plasmodium* infection drives broad modulation of membrane transport, MAPK, and Hippo pathways, including regulatory genes of cell proliferation and tissue homeostasis, as well as upregulation of immune-related genes across different cell types in the *Anopheles* midgut, suggesting a coordinated response to parasite invasion. Previous studies on the impact of naturally occurring, low-level *Plasmodium* infections on vector health and longevity suggested that such infection may enhance olfactory acuity and increase the fitness of *Anopheles* mosquitoes through both anti-aging and reproductive advantages [87]. From an evolutionary perspective, the activation of immune defenses by blood meals prepares mosquitoes to counteract damage from potential pathogens in the blood meal. Furthermore, low-level *Plasmodium* infection may promote pathogen-resistance selection in the general population, potentially improving mosquito survival and thus sustaining population prosperity.

Conclusions and limitations

In this study, we successfully utilized single-cell RNA sequencing to comprehensively characterize the alterations in midgut cell composition and transcriptional profiles across sugar-fed, uninfected blood-fed, and *Plasmodium*-infected *Anopheles* mosquitoes. We identified and described major cell types, including intestinal stem cells/enteroblasts (ISCs/EBs), enteroendocrine cells (EEs), enterocytes (ECs), and cardia cells (CAs), consistent with previous reports in mosquito and fly midguts. Our findings revealed that both blood feeding and *Plasmodium* infection alter the cellular composition and

Langtaosha (LTS) Preprint doi: https://doi.org/10.65215/LTSpreprints.2026.11.21.000397. This version posted November 21, 2026. The copyright holder for this preprint (which was not certified by peer review) is the author/funder. Creative Commons license: CC Attribution-NonCommercial-NoDerivatives 4.0 https://creativecommons.org/licenses/by-nc-nd/4.0

transcriptional landscape of the *Anopheles* midgut, particularly through the differential expression of immune-related genes. Notably, we detected *Plasmodium* transcripts in almost all midgut cell types as early as 24 hours post-blood feeding, suggesting a broad cellular tropism of parasite-vector interactions. Taken together, this study provides critical single-cell-level insights into how blood feeding and *Plasmodium* infection reshape the cellular composition and transcription of the *Anopheles* mosquito midgut, advancing our understanding of the intestinal responses that underpin vector competence.

Nevertheless, this study has limitations that warrant consideration. Due to practical constraints (limited personnel, funding, and access to the *Plasmodium* parasites), this study did not include biological replicates or functional validation. Furthermore, the differential gene expression analysis relied on single-cell observations. While this approach allows for high-resolution mapping of transcriptional changes, it may be subject to pseudoreplication and inflated statistical significance. Therefore, the identified gene signatures should be interpreted as preliminary candidates requiring further validation in future studies.

Abbreviations

ADA	Adenosine deaminase
AMG	Anterior midgut
AMP	Antimicrobial peptide
BP	Biological process
CA	Cardia
CC	Cellular component
CTL	C-type lysozyme
DEG	Differentially expressed gene
Dh	Diuretic hormone receptor
EC	Enterocyte
EE	Enteroendocrine cell
GC	Goblet cell
GO	Gene Ontology
GST	Glutathione S-transferase
Hsp	Heat shock protein
IMD	Immune deficiency
ISC/EB	Intestinal stem cell/enteroblast
JAK-STAT	Janus Kinase-Signal Transducer and Activator of Transcription
KEGG	Kyoto Encyclopedia of Genes and Genomes
Klu	Klumpfuss
MAPK	Mitogen-Activated Protein Kinase
MF	Molecular function
Mhc	Myosin heavy chain
Mlc	Myosin light chain
NCBI	National Center for Biotechnology Information
NPC2	Niemann-Pick type C2

Langtaosha (LTS) Preprint doi: https://doi.org/10.65215/LTSpreprints.2026.11.21.000397. This version posted November 21, 2026. The copyright holder for this preprint (which was not certified by peer review) is the author/funder. Creative Commons license: CC Attribution-NonCommercial-NoDerivatives 4.0 https://creativecommons.org/licenses/by-nc-nd/4.0

PBS	Phosphate-buffered saline
PGRP	Peptidoglycan Recognition Protein
PMG	Posterior midgut
Pros	Prospero
RNAi	RNA interference
RPL19	Ribosomal protein L19
scRNA-Seq	Single-cell RNA sequencing
snRNA-Seq	Single-nucleus RNA sequencing
Tk	Tachykinin
UMAP	Uniform Manifold Approximation and Projection
UMI	Unique Molecular Identifier
WNV	*West Nile* virus

Acknowledgements

We thank the Biosafety Level 2 (BSL-2) and Animal Biosafety Level 2 (ABSL-2) Laboratories of the Institute of Infectious Diseases, Shenzhen Bay Laboratory, for their support and assistance during this research.

Author contributions

Conceived and designed the study: Feng Liu and Jinwen Wang. Performed the experiments: Shan Li, Guanzhen Fan, and Simin Liang. Prepared the materials: Guanzhen Fan and Wenxu Yang. Wrote the paper: Feng Liu, Shan Li, and Guanzhen Fan. Edited the manuscript: Feng Liu, Jinwen Wang, Stephen T. Ferguson, Ming Li, and Zhiyue Lv.

Funding

The research reported in this manuscript was supported by the National Natural Science Foundation of China (Grants 82372289 and 82561128263) and Guangdong Pearl River Funding (Grant No. 2023QN10Y093) awarded to F.L., and Bill & Melinda Gates Foundation INV-061480 awarded to Z.L.

Data availability

The raw sequencing data are available in the NCBI (PRJNA1472872). All relevant data are within the manuscript and its supporting information files. All materials used in this study are available upon request from the corresponding author.

Declarations

Ethics approval and consent to participate

All animals were handled strictly in accordance with the guidelines of the Care and Use of Laboratory Animals of the National Institutes of Health and the Office of Laboratory Animal Welfare, China. The research protocol was approved by the Institutional Animal Care and Use Committee, Department of Laboratory Animal Science, Fudan University, China.

Langtaosha (LTS) Preprint doi: https://doi.org/10.65215/LTSpreprints.2026.11.21.000397. This version posted November 21, 2026. The copyright holder for this preprint (which was not certified by peer review) is the author/funder. Creative Commons license: CC Attribution-NonCommercial-NoDerivatives 4.0 https://creativecommons.org/licenses/by-nc-nd/4.0

Consent for publication

All authors consent to publishing this work.

Competing Interests

The authors declare no competing or financial interests.

Authors' information

[1]School of Grain and Food & Pharmacy, Jiangsu Vocational College of Finance & Economics, Huai'an, 223003, China. [2]Institute of Infectious Diseases, Shenzhen Bay Laboratory, Shenzhen, 518107, China. [3]School of Pharmaceutical Science and Technology, Tianjin University, Tianjin, 300072, China. [4]The State Key Laboratory of Genetic Engineering, School of Life Sciences, Fudan University, Shanghai, 200090, China. [5]Department of Parasitology, Zhongshan School of Medicine, Sun Yat-sen University, Guangzhou, 510080, China. [6]Guangdong Provincial Key Laboratory of Infection Immunity and Inflammation, Shenzhen, China.

References

1. Sinka ME, Pironon S, Massey NC, Longbottom J, Hemingway J, Moyes CL, et al. A new malaria vector in africa: Predicting the expansion range of anopheles stephensi and identifying the urban populations at risk. Proceedings of the National Academy of Sciences. 2020;117: 24900–24908. doi:10.1073/pnas.2003976117

2. Emiru T, Getachew D, Murphy M, Sedda L, Ejigu LA, Bulto MG, et al. Evidence for a role of anopheles stephensi in the spread of drug- and diagnosis-resistant malaria in africa. Nat Med. 2023;29: 3203–3211. doi:10.1038/s41591-023-02641-9

3. Taylor R, Messenger LA, Abeku TA, Clarke SE, Yadav RS, Lines J. Invasive anopheles stephensi in africa: Insights from asia. Trends in Parasitology. 2024;40: 731–743. doi:10.1016/j.pt.2024.06.008

4. Mohammed M, Dziedziech A, Sekar V, Ernest M, Alves E Silva TL, Balan B, et al. Single-Cell Transcriptomics To Define Plasmodium falciparum Stage Transition in the Mosquito Midgut. Microbiology Spectrum. 2023;11: e03671-22. doi:10.1128/spectrum.03671-22

5. Ruberto AA, Bourke C, Merienne N, Obadia T, Amino R, Mueller I. Single-cell RNA sequencing reveals developmental heterogeneity among plasmodium berghei sporozoites. Sci Rep. 2021;11: 4127. doi:10.1038/s41598-021-82914-w

6. Vlachou D, Schlegelmilch T, Runn E, Mendes A, Kafatos FC. The developmental migration of *plasmodium* in mosquitoes. Current Opinion in Genetics & Development. 2006;16: 384–391. doi:10.1016/j.gde.2006.06.012

7. Okuda K, Caroci A de S, Ribolla PEM, de Bianchi AG, Bijovsky AT. Functional morphology of adult female *culex quinquefasciatus* midgut during blood digestion. Tissue and Cell. 2002;34: 210–219. doi:10.1016/S0040-8166(02)00032-0

Langtaosha (LTS) Preprint doi: https://doi.org/10.65215/LTSpreprints.2026.11.21.000397. This version posted November 21, 2026. The copyright holder for this preprint (which was not certified by peer review) is the author/funder. Creative Commons license: CC Attribution-NonCommercial-NoDerivatives 4.0 https://creativecommons.org/licenses/by-nc-nd/4.0

8. Billingsley PF. The Midgut Ultrastructure of Hematophagous Insects. Annual Review of Entomology. 1990; 219–248. doi:10.1146/annurev.en.35.010190.001251

9. Taracena-Agarwal ML, Hixson B, Nandakumar S, Girard-Mejia AP, Chen RY, Huot L, et al. The midgut epithelium of mosquitoes adjusts cell proliferation and endoreplication to respond to physiological challenges. BMC Biol. 2024;22: 22. doi:10.1186/s12915-023-01769-x

10. Billingsley PF, Lehane MJ. Structure and ultrastructure of the insect midgut. In: Lehane MJ, Billingsley PF, editors. Biology of the Insect Midgut. Dordrecht: Springer Netherlands; 1996. pp. 3–30. doi:10.1007/978-94-009-1519-0_1

11. Segrist E, Cherry S. Using Diverse Model Systems to Define Intestinal Epithelial Defenses to Enteric Viral Infections. Cell Host & Microbe. 2020;27: 329–344. doi:10.1016/j.chom.2020.02.003

12. Wegener C, Veenstra JA. Chemical identity, function and regulation of enteroendocrine peptides in insects. Current Opinion in Insect Science. 2015;11: 8–13. doi:10.1016/j.cois.2015.07.003

13. Singh SR, Zeng X, Zheng Z, Hou SX. The adult Drosophila gastric and stomach organs are maintained by a multipotent stem cell pool at the foregut/midgut junction in the cardia (proventriculus). Cell Cycle. 2011;10: 1109–1120. doi:10.4161/cc.10.7.14830

14. Wang S, Huang Y, Wang F, Han Q, Ren N, Wang X, et al. A cell atlas of the adult female Aedes aegypti midgut revealed by single-cell RNA sequencing. Sci Data. 2024;11: 587. doi:10.1038/s41597-024-03432-8

15. Guo X, Yin C, Yang F, Zhang Y, Huang H, Wang J, et al. The Cellular Diversity and Transcription Factor Code of Drosophila Enteroendocrine Cells. Cell Reports. 2019;29: 4172-4185.e5. doi:10.1016/j.celrep.2019.11.048

16. Hung R-J, Hu Y, Kirchner R, Liu Y, Xu C, Comjean A, et al. A cell atlas of the adult Drosophila midgut. Proceedings of the National Academy of Sciences. 2020;117: 1514–1523. doi:10.1073/pnas.1916820117

17. Severo MS, Landry JJM, Lindquist RL, Goosmann C, Brinkmann V, Collier P, et al. Unbiased classification of mosquito blood cells by single-cell genomics and high-content imaging. Proceedings of the National Academy of Sciences. 2018;115: E7568–E7577. doi:10.1073/pnas.1803062115

18. Cui Y, Franz AWE. Heterogeneity of midgut cells and their differential responses to blood meal ingestion by the mosquito, *Aedes aegypti*. Insect Biochemistry and Molecular Biology. 2020;127: 103496. doi:10.1016/j.ibmb.2020.103496

19. Chen T-Y, Raduwan H, Marín-López A, Cui Y, Fikrig E. Zika virus exists in enterocytes and enteroendocrine cells of the aedes aegypti midgut. iScience. 2024;27: 110353. doi:10.1016/j.isci.2024.110353

Langtaosha (LTS) Preprint doi: https://doi.org/10.65215/LTSpreprints.2026.11.21.000397. This version posted November 21, 2026. The copyright holder for this preprint (which was not certified by peer review) is the author/funder. Creative Commons license: CC Attribution-NonCommercial-NoDerivatives 4.0 https://creativecommons.org/licenses/by-nc-nd/4.0

20. Fitzmeyer EA, Dutt TS, Pinaud S, Graham B, Gallichotte EN, Hill JL, et al. A single-cell atlas of the culex tarsalis midgut during west nile virus infection. PLOS Pathogens. 2025;21: e1012855. doi:10.1371/journal.ppat.1012855

21. Yan Y, Verzier LH, Cheung E, Appetecchia F, March S, Craven AR, et al. Mapping plasmodium transitions and interactions in the anopheles female. Nature. 2025; 1–8. doi:10.1038/s41586-025-09653-0

22. Cázares-Raga FE, Chávez-Munguía B, González-Calixto C, Ochoa-Franco AP, Gawinowicz MA, Rodríguez MH, et al. Morphological and proteomic characterization of midgut of the malaria vector *anopheles albimanus* at early time after a blood feeding. Journal of Proteomics. 2014;111: 100–112. doi:10.1016/j.jprot.2014.07.037

23. Ren H, Yang X, Tang H, Wang X, Su Z, Ou Q, et al. Purine nucleoside phosphorylase mediates midgut physiological functions in aedes aegypti by orchestrating uric acid biosynthesis and oxidative stress homeostasis. Insect Science. n/a. doi:10.1111/1744-7917.70155

24. Eilerts DF, Chandrasegaran K, Ajayi OM, Sharma A, Evans O, VanderGiessen M, et al. Hemoglobin in the diet modulates post-blood feeding behavioral rhythms and gene expression in aedes aegypti. bioRxiv. 2025; 2025.08.29.673051. doi:10.1101/2025.08.29.673051

25. Dobin A, Davis CA, Schlesinger F, Drenkow J, Zaleski C, Jha S, et al. STAR: Ultrafast universal RNA-seq aligner. Bioinformatics. 2013;29: 15–21. doi:10.1093/bioinformatics/bts635

26. Liao Y, Smyth GK, Shi W. featureCounts: An efficient general purpose program for assigning sequence reads to genomic features. Bioinformatics. 2014;30: 923–930. doi:10.1093/bioinformatics/btt656

27. Hao Y, Stuart T, Kowalski MH, Choudhary S, Hoffman P, Hartman A, et al. Dictionary learning for integrative, multimodal and scalable single-cell analysis. Nat Biotechnol. 2024;42: 293–304. doi:10.1038/s41587-023-01767-y

28. Cao J, Spielmann M, Qiu X, Huang X, Ibrahim DM, Hill AJ, et al. The single-cell transcriptional landscape of mammalian organogenesis. Nature. 2019;566: 496–502. doi:10.1038/s41586-019-0969-x

29. Waterhouse RM, Kriventseva EV, Meister S, Xi Z, Alvarez KS, Bartholomay LC, et al. Evolutionary dynamics of immune-related genes and pathways in disease-vector mosquitoes. Science. 2007;316: 1738–1743. doi:10.1126/science.1139862

30. Chen C, Wu Y, Li J, Wang X, Zeng Z, Xu J, et al. TBtools-II: A “one for all, all for one” bioinformatics platform for biological big-data mining. Molecular Plant. 2023;16: 1733–1742. doi:10.1016/j.molp.2023.09.010

31. Collins FH, Besansky NJ. Vector Biology and the Control of Malaria in Africa. Science. 1994;264: 1874–1875. doi:10.1126/science.8009215

Langtaosha (LTS) Preprint doi: https://doi.org/10.65215/LTSpreprints.2026.11.21.000397. This version posted November 21, 2026. The copyright holder for this preprint (which was not certified by peer review) is the author/funder. Creative Commons license: CC Attribution-NonCommercial-NoDerivatives 4.0 https://creativecommons.org/licenses/by-nc-nd/4.0

32. Ferguson HM, Read AF. Mosquito appetite for blood is stimulated by plasmodium chabaudi infections in themselves and their vertebrate hosts. Malar J. 2004;3: 12. doi:10.1186/1475-2875-3-12

33. Mathias DK, Jardim JG, Parish LA, Armistead JS, Trinh HV, Kumpitak C, et al. Differential roles of an anopheline midgut GPI-anchored protein in mediating plasmodium falciparum and plasmodium vivax ookinete invasion. Infect Genet Evol. 2014;28: 635–647. doi:10.1016/j.meegid.2014.05.025

34. Vlachou D, Schlegelmilch T, Christophides GK, Kafatos FC. Functional genomic analysis of midgut epithelial responses in anopheles during plasmodium invasion. Curr Biol. 2005;15: 1185–1195. doi:10.1016/j.cub.2005.06.044

35. Fitzmeyer EA, Dutt TS, Pinaud S, Graham B, Gallichotte EN, Hill JL, et al. A single-cell atlas of the Culex tarsalis midgut during West Nile virus infection. PLOS Pathogens. 2025;21: e1012855. doi:10.1371/journal.ppat.1012855

36. Lavazec C, Bonnet S, Thiery I, Boisson B, Bourgouin C. *cpbAg1* encodes an active carboxypeptidase B expressed in the midgut of *Anopheles gambiae*. Insect Molecular Biology. 2005;14: 163–174. doi:10.1111/j.1365-2583.2004.00541.x

37. Vial T, Lopez-Maestre H, Couderc E, Pinaud S, Howick V, Akorli J, et al. Single-cell transcriptional landscapes of *aedes aegypti* midgut and fat body after a bloodmeal. Cell Genomics. 2025; 100924. doi:10.1016/j.xgen.2025.100924

38. Sodja A, Fujioka H, Lemos FJA, Donnelly-Doman M, Jacobs-Lorena M. Induction of actin gene expression in the mosquito midgut by blood ingestion correlates with striking changes of cell shape. Journal of Insect Physiology. 2007;53: 833–839. doi:10.1016/j.jinsphys.2007.03.017

39. Dana AN, Hong YS, Kern MK, Hillenmeyer ME, Harker BW, Lobo NF, et al. Gene expression patterns associated with blood-feeding in the malaria mosquito anopheles gambiae. BMC Genomics. 2005;6: 5. doi:10.1186/1471-2164-6-5

40. Padrón A, Molina-Cruz A, Quinones M, Ribeiro JM, Ramphul U, Rodrigues J, et al. In depth annotation of the anopheles gambiae mosquito midgut transcriptome. BMC Genomics. 2014;15: 636. doi:10.1186/1471-2164-15-636

41. Sanders HR, Evans AM, Ross LS, Gill SS. Blood meal induces global changes in midgut gene expression in the disease vector, *Aedes aegypti*. Insect Biochemistry and Molecular Biology. 2003;33: 1105–1122. doi:10.1016/S0965-1748(03)00124-3

42. Cui Y, Niu G, Li VL, Wang X, Li J. Analysis of blood-induced Anopheles gambiae midgut proteins and sexual stage Plasmodium falciparum interaction reveals mosquito genes important for malaria transmission. Sci Rep. 2020;10: 14316. doi:10.1038/s41598-020-71186-5

43. Gendrin M, Rodgers FH, Yerbanga RS, Ouédraogo JB, Basáñez M-G, Cohuet A, et al. Antibiotics in ingested human blood affect the mosquito microbiota and capacity to transmit

Langtaosha (LTS) Preprint doi: https://doi.org/10.65215/LTSpreprints.2026.11.21.000397. This version posted November 21, 2026. The copyright holder for this preprint (which was not certified by peer review) is the author/funder. Creative Commons license: CC Attribution-NonCommercial-NoDerivatives 4.0 https://creativecommons.org/licenses/by-nc-nd/4.0

malaria. Nature Communications. 2015;6: 5921. doi:10.1038/ncomms6921

44. Hixson B, Bing X-L, Yang X, Bonfini A, Nagy P, Buchon N. A transcriptomic atlas of aedes aegypti reveals detailed functional organization of major body parts and gut regional specializations in sugar-fed and blood-fed adult females. Elife. 2022;11: e76132. doi:10.7554/eLife.76132

45. Barletta A-BF, Smith JC, Burkart E, Bondarenko S, Sharakhov IV, Criscione F, et al. Mosquito midgut stem cell cellular defense response limits plasmodium parasite infection. Nat Commun. 2024;15: 1422. doi:10.1038/s41467-024-45550-2

46. Benoit JB, Lopez-Martinez G, Patrick KR, Phillips ZP, Krause TB, Denlinger DL. Drinking a hot blood meal elicits a protective heat shock response in mosquitoes. Proceedings of the National Academy of Sciences. 2011;108: 8026–8029. doi:10.1073/pnas.1105195108

47. Benoit JB, Lopez-Martinez G, Phillips ZP, Patrick KR, Denlinger DL. Heat shock proteins contribute to mosquito dehydration tolerance. Journal of Insect Physiology. 2010;56: 151–156. doi:10.1016/j.jinsphys.2009.09.012

48. Alves E Silva TL, Canepa GE, Sweeney B, Hessab Alvarenga P, Zhao M, Vega-Rodríguez J, et al. The heat shock protein Hsc70-3 mediates an anti-apoptotic response critical for plasmodium evasion of anopheles gambiae immunity. Microbiol Spectr. 2023;11: e0094023. doi:10.1128/spectrum.00940-23

49. Zurovec M, Dolezal T, Gazi M, Pavlova E, Bryant PJ. Adenosine deaminase-related growth factors stimulate cell proliferation in drosophila by depleting extracellular adenosine. Proc Natl Acad Sci U S A. 2002;99: 4403–4408. doi:10.1073/pnas.062059699

50. Ren F, Wang B, Yue T, Yun E-Y, Ip YT, Jiang J. Hippo signaling regulates drosophila intestine stem cell proliferation through multiple pathways. Proc Natl Acad Sci U S A. 2010;107: 21064–21069. doi:10.1073/pnas.1012759107

51. Huang J, Wu S, Barrera J, Matthews K, Pan D. The hippo signaling pathway coordinately regulates cell proliferation and apoptosis by inactivating yorkie, the drosophila homolog of YAP. Cell. 2005;122: 421–434. doi:10.1016/j.cell.2005.06.007

52. Wang B, Pakpour N, Napoli E, Drexler A, Glennon EKK, Surachetpong W, et al. Anopheles stephensi p38 MAPK signaling regulates innate immunity and bioenergetics during plasmodium falciparum infection. Parasit Vectors. 2015;8: 424. doi:10.1186/s13071-015-1016-x

53. Huang Z, Tian Z, Zhao Y, Zhu F, Liu W, Wang X. MAPK signaling pathway is essential for female reproductive regulation in the cabbage beetle, colaphellus bowringi. Cells. 2022;11: 1602. doi:10.3390/cells11101602

54. Molina JR, Adjei AA. The ras/raf/MAPK pathway. Journal of Thoracic Oncology. 2006;1: 7–9. doi:10.1016/S1556-0864(15)31506-9

Langtaosha (LTS) Preprint doi: https://doi.org/10.65215/LTSpreprints.2026.11.21.000397. This version posted November 21, 2026. The copyright holder for this preprint (which was not certified by peer review) is the author/funder. Creative Commons license: CC Attribution-NonCommercial-NoDerivatives 4.0 https://creativecommons.org/licenses/by-nc-nd/4.0

948 55. Xing J, Ginty DD, Greenberg ME. Coupling of the RAS-MAPK pathway to gene activation by
949 RSK2, a growth factor-regulated CREB kinase. Science. 1996;273: 959–963.
950 doi:10.1126/science.273.5277.959

951 56. Lopez AD, Debnath T, Pinch M, Hansen IA. Phosphoproteomics analyses of aedes aegypti fat
952 body reveals blood meal-induced signaling and metabolic pathways. Heliyon. 2024;10.
953 doi:10.1016/j.heliyon.2024.e40060

954 57. Bi B, Yuan Y, Zhao Y, He M, Song H, Kong L, et al. Effect of crowding stress on growth
955 performance, the antioxidant system and humoral immunity in hybrid sturgeon. Aquaculture
956 Reports. 2023;28: 101468. doi:10.1016/j.aqrep.2023.101468

957 58. Wang D, Guo S, He H, Gong L, Cui H. Gut Microbiome and Serum Metabolome Analyses
958 Identify Unsaturated Fatty Acids and Butanoate Metabolism Induced by Gut Microbiota in
959 Patients With Chronic Spontaneous Urticaria. Front Cell Infect Microbiol. 2020;10.
960 doi:10.3389/fcimb.2020.00024

961 59. Yahsi B, Gunaydin G. Immunometabolism – The Role of Branched-Chain Amino Acids. Front
962 Immunol. 2022;13. doi:10.3389/fimmu.2022.886822

963 60. Yan F, Zhang Q, Shi K, Zhang Y, Zhu B, Bi Y, et al. Gut microbiota dysbiosis with hepatitis B
964 virus liver disease and association with immune response. Front Cell Infect Microbiol. 2023;13.
965 doi:10.3389/fcimb.2023.1152987

966 61. Zhang Z, Fan Z, Yi M, Liu Z, Ke X, Gao F, et al. Characterization of the core gut microbiota of
967 Nile tilapia (Oreochromis niloticus): indication of a putative novel Cetobacterium species and
968 analysis of its potential function on nutrition. Arch Microbiol. 2022;204: 690.
969 doi:10.1007/s00203-022-03301-1

970 62. Mu X, Lin Z, Sun Y, Chen L, Lv Q, Ji C, et al. Aedes albopictus salivary adenosine deaminase
971 is an immunomodulatory factor facilitating dengue virus replication. Sci Rep. 2023;13: 16660.
972 doi:10.1038/s41598-023-43751-1

973 63. Waterhouse RM, Lazzaro BP, Sackton TB. Characterization of Insect Immune Systems from
974 Genomic Data. In: Sandrelli F, Tettamanti G, editors. Immunity in Insects. New York, NY:
975 Springer US; 2020. pp. 3–34. doi:10.1007/978-1-0716-0259-1_1

976 64. Blandin S, Shiao S-H, Moita LF, Janse CJ, Waters AP, Kafatos FC, et al. Complement-like
977 protein TEP1 is a determinant of vectorial capacity in the malaria vector Anopheles gambiae.
978 Cell. 2004;116: 661–670. doi:10.1016/s0092-8674(04)00173-4

979 65. Vasta GR. Roles of galectins in infection. Nat Rev Microbiol. 2009;7: 424–438.
980 doi:10.1038/nrmicro2146

981 66. Vasta GR, Ahmed H, Nita-Lazar M, Banerjee A, Pasek M, Shridhar S, et al. Galectins as
982 self/non-self recognition receptors in innate and adaptive immunity: An unresolved paradox.
983 Front Immunol. 2012;3. doi:10.3389/fimmu.2012.00199

Langtaosha (LTS) Preprint doi: https://doi.org/10.65215/LTSpreprints.2026.11.21.000397. This version posted November 21, 2026. The copyright holder for this preprint (which was not certified by peer review) is the author/funder. Creative Commons license: CC Attribution-NonCommercial-NoDerivatives 4.0 https://creativecommons.org/licenses/by-nc-nd/4.0

67. Maillet F, Bischoff V, Vignal C, Hoffmann J, Royet J. The Drosophila Peptidoglycan Recognition Protein PGRP-LF Blocks PGRP-LC and IMD/JNK Pathway Activation. Cell Host & Microbe. 2008;3: 293–303. doi:10.1016/j.chom.2008.04.002

68. Zaidman-Rémy A, Hervé M, Poidevin M, Pili-Floury S, Kim M-S, Blanot D, et al. The drosophila amidase PGRP-LB modulates the immune response to bacterial infection. Immunity. 2006;24: 463–473. doi:10.1016/j.immuni.2006.02.012

69. Agaisse H, Perrimon N. The roles of JAK/STAT signaling in Drosophila immune responses. Immunol Rev. 2004;198: 72–82. doi:10.1111/j.0105-2896.2004.0133.x

70. Bang IS. JAK/STAT signaling in insect innate immunity. Entomological Research. 2019;49: 339–353. doi:10.1111/1748-5967.12384

71. Blair CD. Mosquito RNAi is the major innate immune pathway controlling arbovirus infection and transmission. Future Microbiology. 2011;6: 265–277. doi:10.2217/fmb.11.11

72. Dennison NJ, BenMarzouk-Hidalgo OJ, Dimopoulos G. MicroRNA-regulation of *anopheles gambiae* immunity to *plasmodium falciparum* infection and midgut microbiota. Developmental & Comparative Immunology. 2015;49: 170–178. doi:10.1016/j.dci.2014.10.016

73. Barletta ABF, Barillas-Mury C, Molina-Cruz A. Mosquito immune responses to Plasmodium parasites that limit malaria transmission. Cell Mol Life Sci. 2025;82: 143. doi:10.1007/s00018-025-05667-z

74. Liu H, Xu J, Wang L, Guo P, Tang Z, Sun X, et al. Serpin-1a and serpin-6 regulate the Toll pathway immune homeostasis by synergistically inhibiting the Spätzle-processing enzyme CLIP2 in silkworm, Bombyx mori. PLOS Pathogens. 2023;19: e1011740. doi:10.1371/journal.ppat.1011740

75. Zhang R, Kang Z, Dong S, Shangguan D, Shoukat RF, Zhang J, et al. Boosting the efficacy of fungal biocontrol: miRNA339-5p-mediated mosquito immunity regulation. Pest Management Science. 2025;81: 1727–1739. doi:10.1002/ps.8572

76. Cerenius L, Söderhäll K. The prophenoloxidase-activating system in invertebrates. Immunol Rev. 2004;198: 116–126. doi:10.1111/j.0105-2896.2004.00116.x

77. Ligoxygakis P, Pelte N, Hoffmann JA, Reichhart J-M. Activation of Drosophila Toll during fungal infection by a blood serine protease. Science. 2002;297: 114–116. doi:10.1126/science.1072391

78. Arya SK, Harrison DA, Palli SR. Cellular and functional heterogeneity of fall armyworm (Spodoptera frugiperda) midgut: a single-cell RNA sequencing analysis. J Pest Sci. 2024 [cited 6 Jan 2025]. doi:10.1007/s10340-024-01828-4

79. Hung R-J, Hu Y, Kirchner R, Liu Y, Xu C, Comjean A, et al. A cell atlas of the adult drosophila midgut. Proc Natl Acad Sci U S A. 2020;117: 1514–1523. doi:10.1073/pnas.1916820117

Langtaosha (LTS) Preprint doi: https://doi.org/10.65215/LTSpreprints.2026.11.21.000397. This version posted November 21, 2026. The copyright holder for this preprint (which was not certified by peer review) is the author/funder. Creative Commons license: CC Attribution-NonCommercial-NoDerivatives 4.0 https://creativecommons.org/licenses/by-nc-nd/4.0

80. Wang S, Huang Y, Wang F, Han Q, Ren N, Wang X, et al. A cell atlas of the adult female aedes aegypti midgut revealed by single-cell RNA sequencing. Sci Data. 2024;11: 587. doi:10.1038/s41597-024-03432-8

81. Xia J, Fei S, Huang Y, Lai W, Yu Y, Liang L, et al. Single-nucleus sequencing of silkworm larval midgut reveals the immune escape strategy of BmNPV in the midgut during the late stage of infection. Insect Biochemistry and Molecular Biology. 2024;164: 104043. doi:10.1016/j.ibmb.2023.104043

82. Arya SK, Harrison DA, Palli SR. Cellular and functional heterogeneity of fall armyworm (Spodoptera frugiperda) midgut: a single-cell RNA sequencing analysis. Journal of Pest Science. 2025;98: 987–1002. doi:10.1007/s10340-024-01828-4

83. Awais MM, Fei S, Xia J, Feng M, Sun J. Insights into midgut cell types and their crucial role in antiviral immunity in the lepidopteran model bombyx mori. Front Immunol. 2024;15. doi:10.3389/fimmu.2024.1349428

84. Soghigian J, Sither C, Justi SA, Morinaga G, Cassel BK, Vitek CJ, et al. Phylogenomics reveals the history of host use in mosquitoes. Nature Communications. 2023;14: 6252. doi:10.1038/s41467-023-41764-y

85. Johnson RM, Cozens DW, Ferdous Z, Armstrong PM, Brackney DE. Increased blood meal size and feeding frequency compromise aedes aegypti midgut integrity and enhance dengue virus dissemination. PLOS Neglected Tropical Diseases. 2023;17: e0011703. doi:10.1371/journal.pntd.0011703

86. Okuda K, de Almeida F, Mortara RA, Krieger H, Marinotti O, Tania Bijovsky A. Cell death and regeneration in the midgut of the mosquito, *Culex quinquefasciatus*. Journal of Insect Physiology. 2007;53: 1307–1315. doi:10.1016/j.jinsphys.2007.07.005

87. Carr AL, Rinker DC, Dong Y, Dimopoulos G, Zwiebel LJ. Transcriptome profiles of anopheles gambiae harboring natural low-level plasmodium infection reveal adaptive advantages for the mosquito. Scientific Reports. 2021;11: 22578. doi:10.1038/s41598-021-01842-x

Table 1. The 6 cell types identified in the female midgut of An. stephensi with marker genes from *Drosophila melanogaster* and *Ae. agypti*.

Langtaosha (LTS) Preprint doi: https://doi.org/10.65215/LTSpreprints.2026.11.21.000397. This version posted November 21, 2026. The copyright holder for this preprint (which was not certified by peer review) is the author/funder. Creative Commons license: CC Attribution-NonCommercial-NoDerivatives 4.0 https://creativecommons.org/licenses/by-nc-nd/4.0

		Non-blood		Blood-fed		Infected blood-fed	
Cell type	Cell markers	Cell No.	Prop. (%)	Cell No.	Prop. (%)	Cell No.	Prop. (%)
ISC/EB	Tk, Delta, Klu	1,989	37.18	1,844	25.48	2,692	33.88
EE	Pros, NPF	149	2.79	285	3.94	1,014	12.76
CA	Gambicin, Tret1, CTL	948	17.72	1,428	19.73	952	11.98
EC	Nubbin	62	1.16	197	2.72	83	1.04
EC-like_1	trypsin-1, trypsin-7	71	1.33	3,482	48.12	3,205	40.33
EC-like_2	CAH2, Nha1, AQPcic, AQPAn.G, trypsin-5	2,130	39.82	0	0.00	0	0.00

Langtaosha (LTS) Preprint doi: https://doi.org/10.65215/LTSpreprints.2026.11.21.000397. This version posted November 21, 2026. The copyright holder for this preprint (which was not certified by peer review) is the author/funder. Creative Commons license: CC Attribution-NonCommercial-NoDerivatives 4.0 https://creativecommons.org/licenses/by-nc-nd/4.0

1068 Table 2. The 19 clusters identified in the female midgut of *An. stephensi*

Cell type	Cell marker	Sugar-fed		Blood-fed		Infected blood-fed	
		Cell No.	Prop. (%)	Cell No.	Prop. (%)	Cell No.	Prop. (%)
ISC/EB-1	Tk, Delta, E(spl)m3-HLH	110	2.06	400	5.53	432	5.44
ISC/EB-2	Tk, Delta, E(spl)m3-HLH	1	0.02	248	3.43	368	4.63
ISC/EB-3	Tk, Klu	1,417	26.49	981	13.56	1,206	15.18
ISC/EB-4	Tk, Delta, Klu, E(spl)m3-HLH	326	6.09	162	2.24	301	3.79
ISC/EB-5	Tk, Klu	135	2.52	53	0.73	385	4.85
EE-1	Dh31, NPF, Pros, Tachykinin	49	0.92	92	1.27	288	3.62
EE-2	CCHa2, NPF, Pros	35	0.65	52	0.72	213	2.68
EE-3	Pros, Tachykinin, Orco	65	1.22	141	1.95	513	6.46
CA-1	Gambicin, Tret1, CTL	61	1.14	454	6.27	245	3.08
CA-2	Gambicin, Tret1	887	16.58	974	13.46	707	8.90
EC	nub	62	1.16	197	2.72	83	1.04
EC-like_1-1	trypsin-1, trypsin-7	0	0.00	304	4.20	182	2.29
EC-like_1-2	trypsin-1, trypsin-7	0	0.00	1,324	18.30	1,469	18.49
EC-like_1-3	trypsin-1, trypsin-7	0	0.00	260	3.59	294	3.70
EC-like_1-4	trypsin-1, trypsin-7, lipase-H	43	0.80	517	7.14	606	7.63
EC-like_1-5	trypsin-1, trypsin-7	28	0.52	1,077	14.88	654	8.23
EC-like_2-1	trypsin-5, AQPcic, AQPAn.G	315	5.89	0	0.00	0	0.00
EC-like_2-2	trypsin-5, AQPcic, AQPAn.G	1,448	27.07	0	0.00	0	0.00
EC-like_2-3	trypsin-5, cp-like	367	6.86	0	0.00	0	0.00

1069

Langtaosha (LTS) Preprint doi: https://doi.org/10.65215/LTSpreprints.2026.11.21.000397. This version posted November 21, 2026. The copyright holder for this preprint (which was not certified by peer review) is the author/funder. Creative Commons license: CC Attribution-NonCommercial-NoDerivatives 4.0 https://creativecommons.org/licenses/by-nc-nd/4.0

Figure legends

Fig 1. Oocyst quantification in *An. stephensi* midgut following *P. berghei* infection. (A) Schematic showing the procedure for Plasmodium infection in *An. stephensi* midgut; (B) Number of oocysts counted in the midguts of mosquitoes fed an infected blood meal. Each data point represents one midgut. Zero values are included.

Fig 2. Annotation of midgut cell clusters of mosquitoes under different feeding conditions. (A) DotPlot showing the proportion of midgut cells (represented by circle size) expressing marker genes and mean marker gene expression levels (represented by circle color) in each cluster; (B) Integrated UMAP based on the datasets obtained from the midguts of sugar-fed, blood-fed, and infected blood-fed mosquitoes showing cell-specific labeling; (C) UMAPs of midgut cells of sugar-fed mosquitoes; (D) UMAPs of midgut cells of blood-fed mosquitoes; (E) UMAPs of midgut cells of infected blood-fed mosquitoes; (F-K) Marker genes of each cluster in integrated scRNA-seq datasets of An. stephensi midguts.

Fig 3. Subclusters of different cell types in the midguts of Anopheles mosquitoes fed different diets. Canonical and statistically identified marker genes of different cell clusters were listed on the right side of the dot plot. Each cell type was color-coded at the top. The clustering resolution is 0.7.

Fig 4. Transcript profiles of blood-fed and sugar-fed An. stephensi midgut cells. (A) GO enrichment of DEGs between blood-fed and sugar-fed midguts; (B) DEGs between blood-fed and sugar-fed midguts; the x-axis indicates the difference in the proportion of cells expressing genes between the blood-fed and sugar-fed midguts; y-axis indicates the average transcriptional fold change of genes between the blood-fed and sugar-fed midgut cells. The dot sizes of specific genes of particular interest were enlarged to increase their visibility. (C) Transcriptional abundance of signature genes predominantly expressed in EC-like cluster, which are actively involved in carbohydrate digestion. (D) Transcription counts of three Niemann-Pick type C2 genes in the blood-fed and sugar-fed EE cell populations.

Fig 5. Distribution of mosquito midgut cell clusters sampled 24 hours post-infected-blood feeding. (A) Number of cells with dual-read host-parasite barcodes in each cell cluster and (B) proportion of *Plasmodium* cells with dual-read host-parasite barcodes in each cell cluster.

Fig 6. Transcript profiles of infected blood-fed and uninfected blood-fed An. stephensi midgut cells. (A) DEGs between infected blood-fed and uninfected blood-fed midgut cells. The x-axis indicates the difference in cell ratio for genes expressed between the blood-fed and sugar-fed midgut. The y-axis indicates the average transcriptional fold changes of genes between the blood-fed and sugar-fed midgut cells. (B) KEGG pathway enrichment of DEGs between uninfected blood-fed and sugar-fed midgut. The point size indicates the number of enriched genes, and the color indicates the main class of KEGG pathway. (C) KEGG pathway enrichment of DEGs between infected blood-fed and uninfected blood-fed midgut. The point size indicates the number of enriched genes, and the color indicates the main class of KEGG pathway.

Fig 7. Transcriptional abundance of immune genes from different pathways across various midgut cell

Langtaosha (LTS) Preprint doi: https://doi.org/10.65215/LTSpreprints.2026.11.21.000397. This version posted November 21, 2026. The copyright holder for this preprint (which was not certified by peer review) is the author/funder. Creative Commons license: CC Attribution-NonCommercial-NoDerivatives 4.0 https://creativecommons.org/licenses/by-nc-nd/4.0

clusters. The names of each pathway are listed on the right side of the genes, and their VectorBase IDs (last five digits) are placed on the left. The heatmap displays scaled average expression of specific genes within each cell cluster of the midgut in mosquitoes fed with uninfected blood and infected blood. The genes were identified through homology-based annotation by BLAST against ImmunoDB.

Fig S1. Doublet identification in scRNA-seq data from *An. stephensi* midgut samples. UMAP visualization of doublet detection for each sample under different experimental conditions. (A) sugar-fed sample, (B) blood meal sample, and (C) *Plasmodium berghei*-infected blood meal sample. Singlets and doublets are shown in yellow and red, respectively. Doublets were identified using DoubletFinder and removed prior to downstream analysis.

Fig S2. Summary of scRNA-seq data of *An. stephensi* after filtering low-quality cells using CeleScope (version v1.9.0) with default parameters. (A) Distribution of the number of genes in each sample after data filtering. (B) Distribution of the number of UMIs in each sample after data filtering. (C) Distribution of the mitochondrial gene percentage in each sample after data filtering.

Fig S3. Lineage of cellular differentiation pathways constructed using Monocle 3. ISC/EB were used to identify and order the root cells that served as the starting point of the pseudotime analysis. The color gradient indicates the pseudotime progression. The specific name was placed near each cell cluster. Dashed lines of different colors were used to manually indicate the developmental trajectory of different cell types.

Fig S4. Gene ontology enrichment analysis and differentially expressed genes of EC cells identified between infected-fed and uninfected blood-fed mosquitoes: A) GO enrichment of upregulated genes in the EC cells of infected blood-fed mosquitoes; B) DEGs between EC cells of infected and uninfected blood-fed mosquitoes. The dot sizes of specific genes of particular interest were enlarged to increase their visibility.

Fig S5. Gene ontology enrichment analysis and differentially expressed genes of EE cells identified between infected blood-fed and uninfected blood-fed mosquitoes: A) GO enrichment of upregulated genes in the EE cells of infected blood-fed mosquitoes; B) DEGs between EE cells of infected and uninfected blood-fed mosquitoes.

Fig S6. Average transcriptional counts of *RPL19* in each midgut sample.

Table S1. Summary of the number of cells in each sample before and after data filtering.

Table S2. Sequencing metrics of the single-cell RNA-sequencing libraries used in this study, including the total reads for each sample; the median number of genes per sample; the median number of genes per cell in each sample; and the median number of UMIs per cell in each sample.

Table S3. The upregulated and downregulated genes in blood-fed mosquitoes compared to uninfected blood-fed controls (fold change $\geqslant$ 2, adjusted p value < 0.05).

Table S4. The upregulated and downregulated genes in EC-like_1 of blood-fed mosquitoes compared

Langtaosha (LTS) Preprint doi: https://doi.org/10.65215/LTSpreprints.2026.11.21.000397. This version posted November 21, 2026. The copyright holder for this preprint (which was not certified by peer review) is the author/funder. Creative Commons license: CC Attribution-NonCommercial-NoDerivatives 4.0 https://creativecommons.org/licenses/by-nc-nd/4.0

1146 to uninfected blood-fed controls (fold change ⩾ 2, adjusted p-value < 0.05).

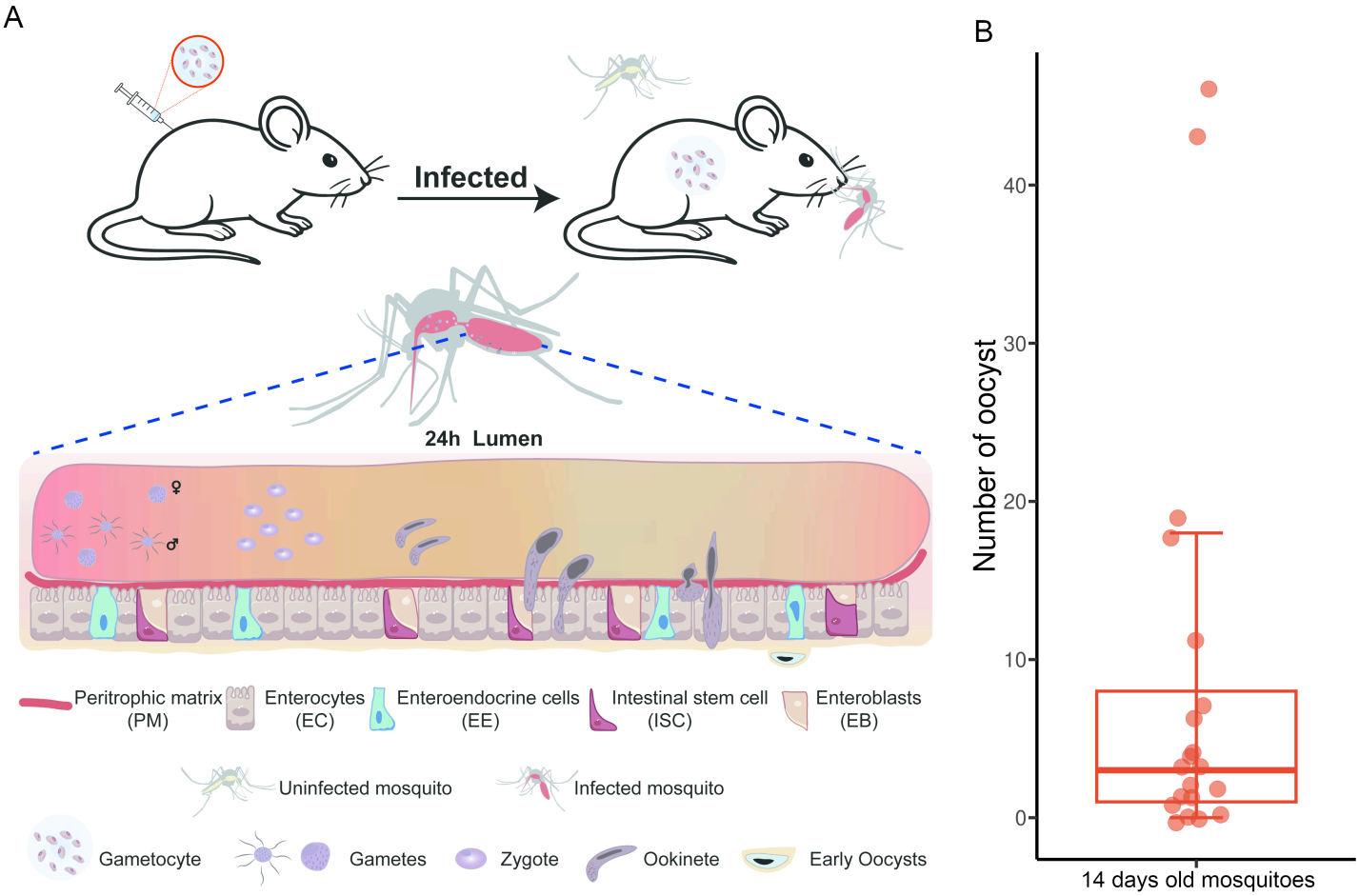
1147 Table S5. The upregulation of genes involved in innate immunity and cellular homeostasis in EE cells
1148 in the midgut of blood-fed mosquitoes compared to sugar-fed controls (adjusted p-value <0.05).

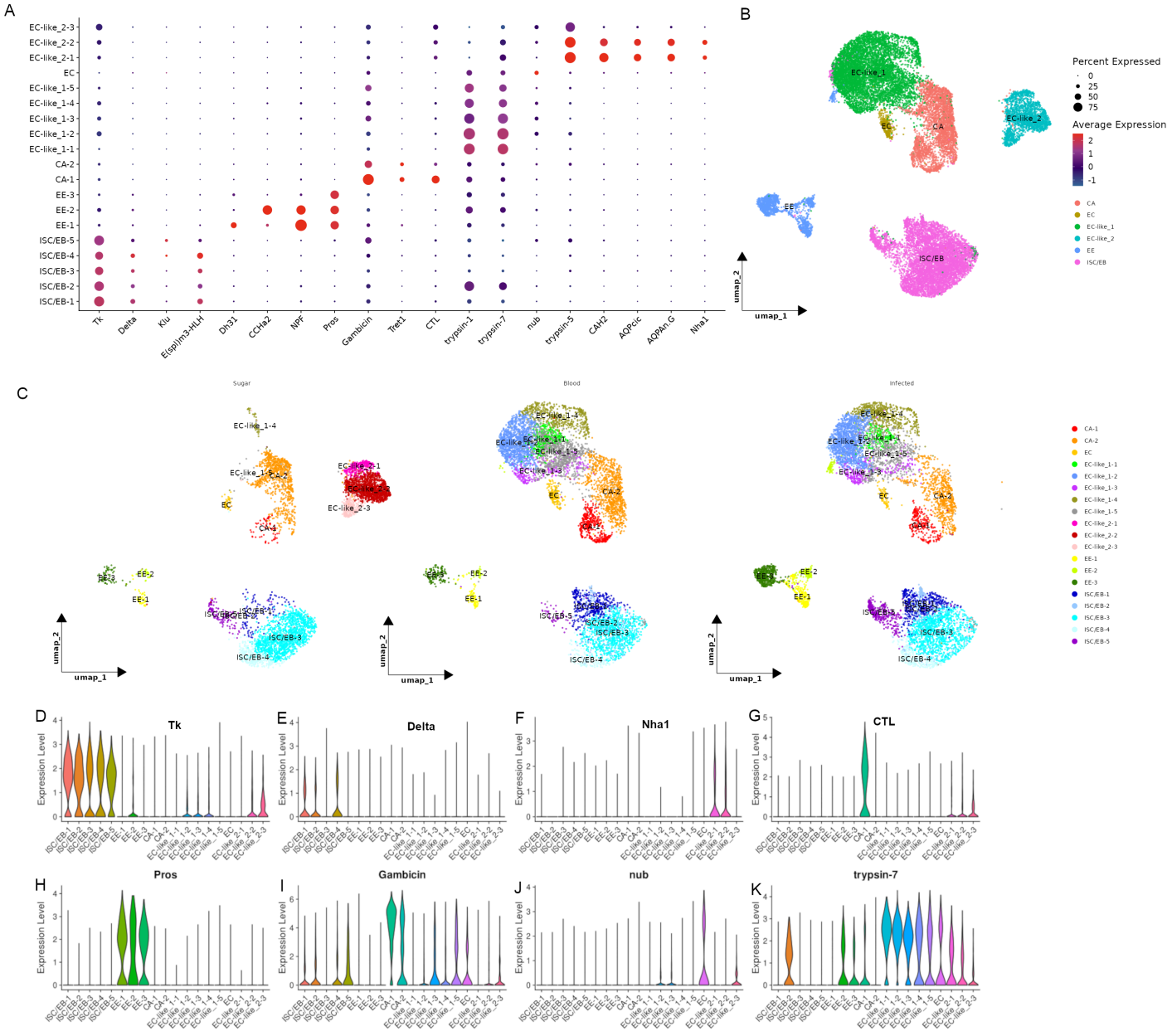
1149 Table S6. The upregulated and downregulated genes in CA of blood-fed mosquitoes compared to
1150 uninfected blood-fed controls (fold change ⩾ 2, adjusted p-value <0.05).

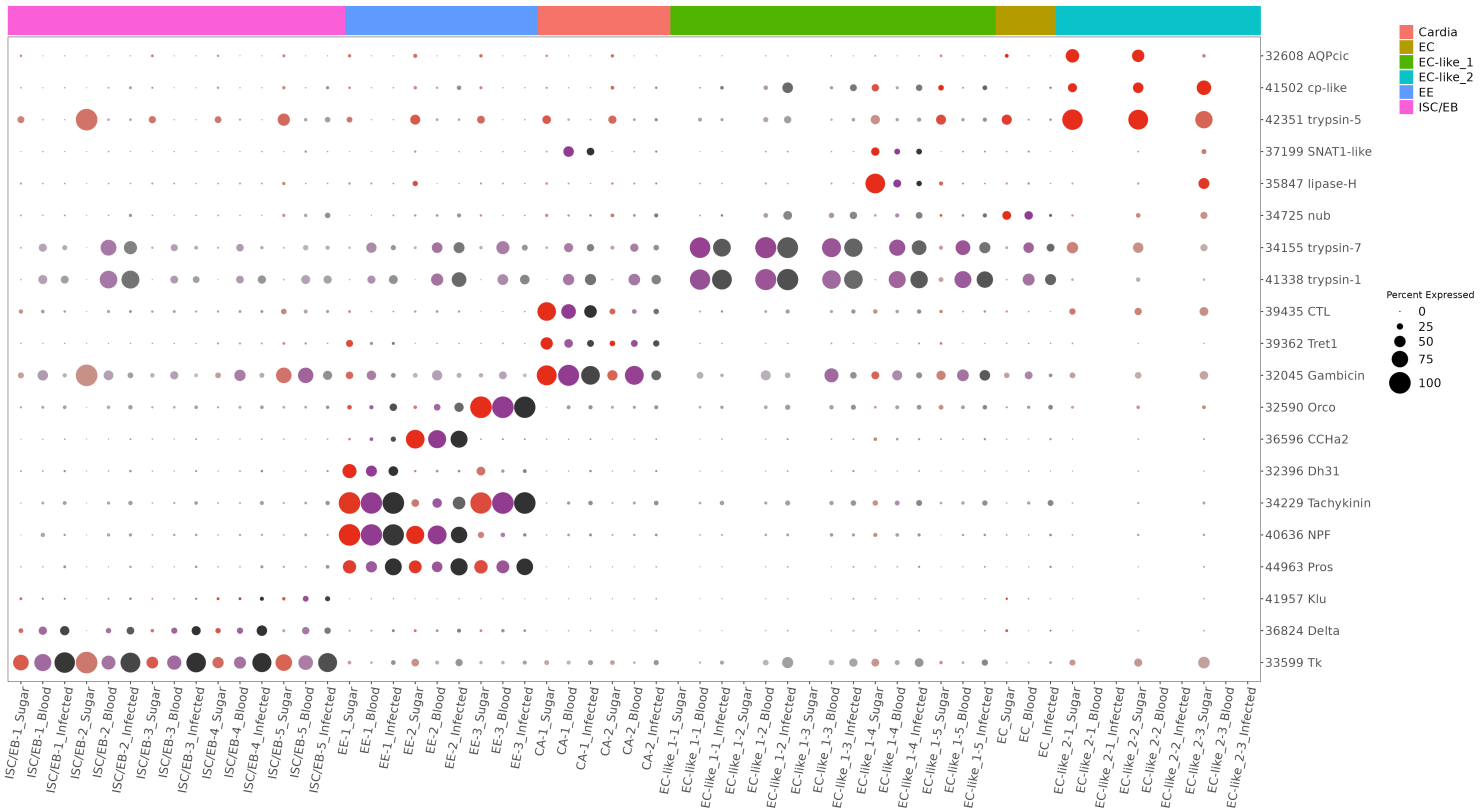
1151 Table S7. The upregulated and downregulated genes in blood-fed mosquitoes compared to uninfected
1152 blood-fed controls (fold change ⩾2, adjusted p-value <0.05).

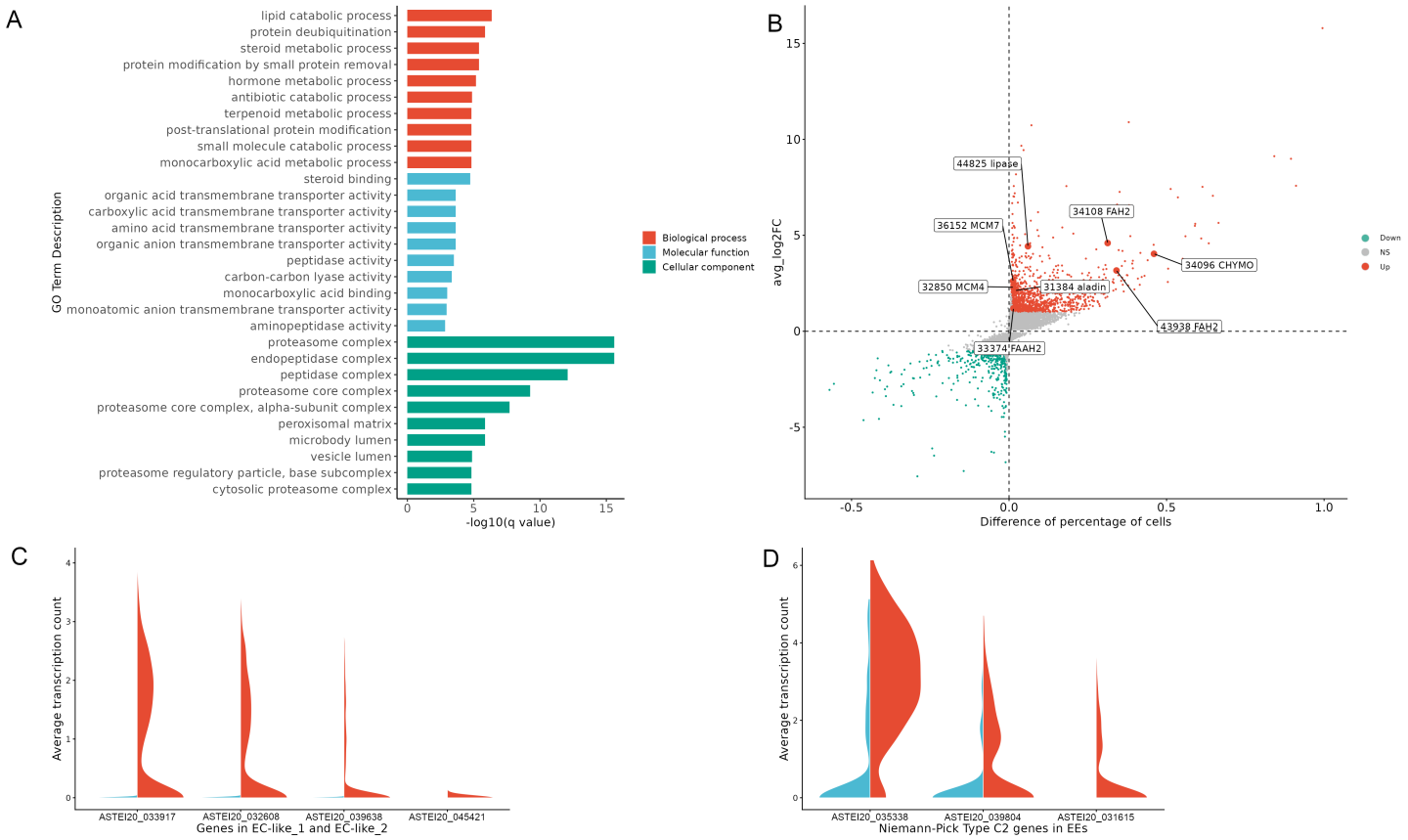
1153 Table S8. Identification of signaling pathways involved in transcriptional modulation of the mosquito
1154 midgut based on the upregulated genes induced by *Plasmodium* infection.

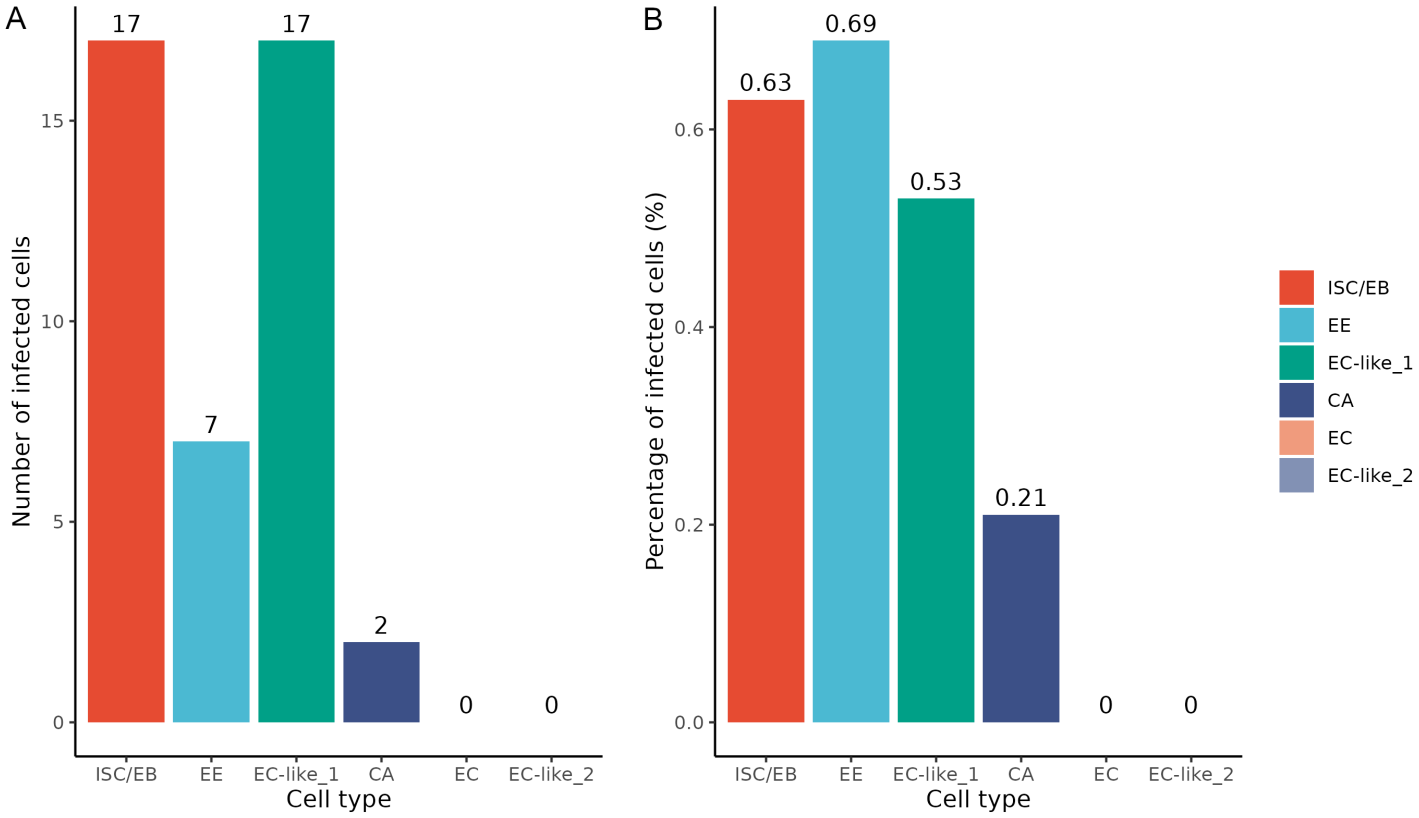
1155 Table S9. Cell-level differential expression for the ribosomal protein gene RPL19 in pairwise
1156 comparisons across three experimental conditions using the FindMarkers function of Seurat
1157 pipeline.

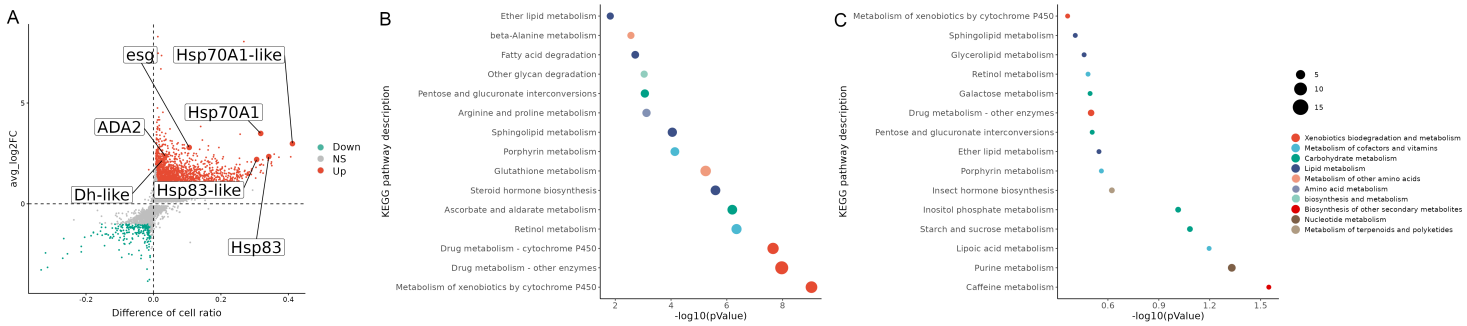

A
Infected
24h Lumen
♀
♂
Peritrophic matrix (PM)
Enterocytes (EC)
Enteroendocrine cells (EE)
Intestinal stem cell (ISC)
Enteroblasts (EB)
Uninfected mosquito
Infected mosquito
Gametocyte
Gametes
Zygote
Ookinete
Early Oocysts
B
Number of oocyst
0
10
20
30
40
14 days old mosquitoes

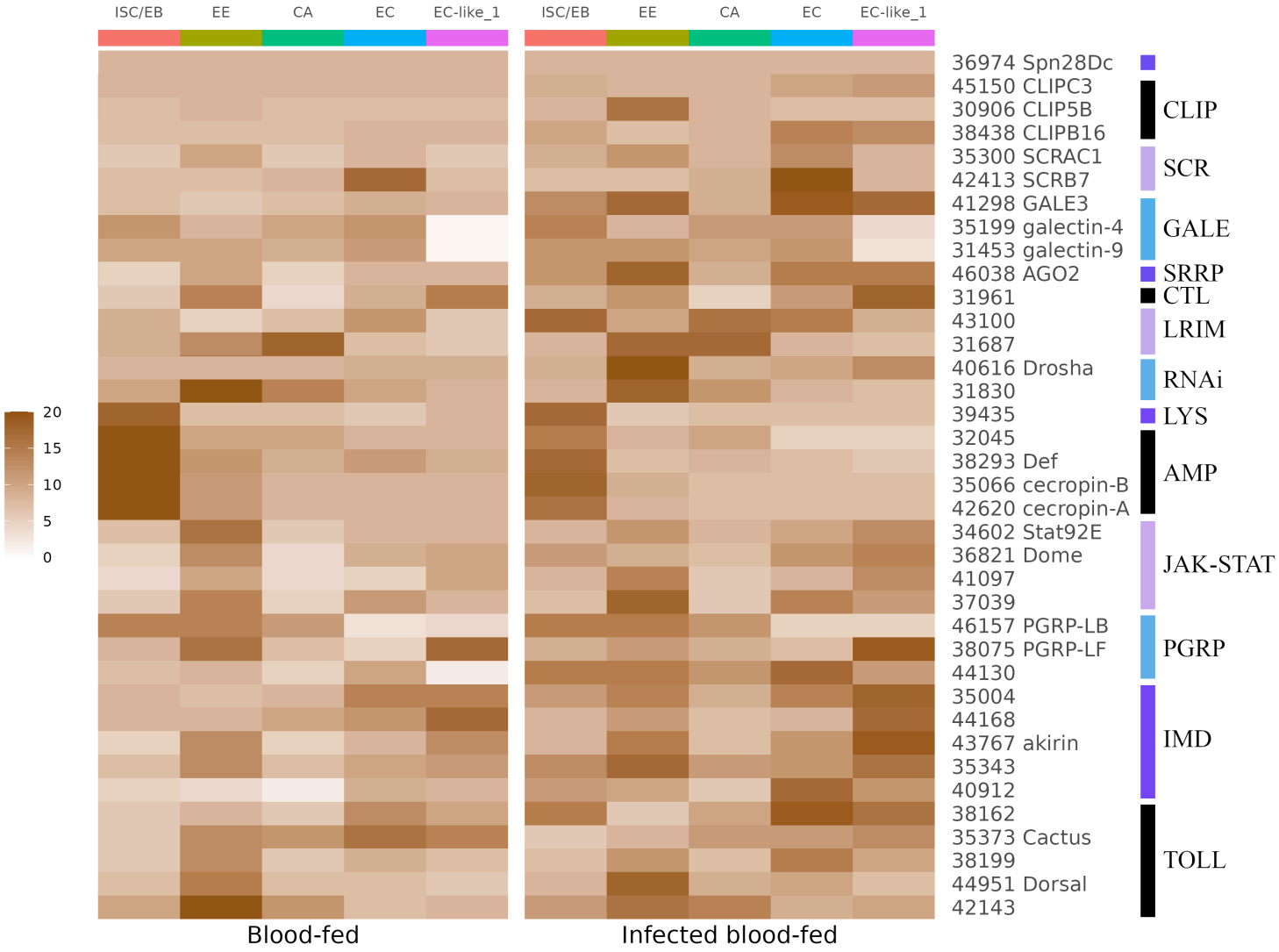

A
EC-like_2-3
EC-like_2-2
EC-like_2-1
EC
EC-like_1-5
EC-like_1-4
EC-like_1-3
EC-like_1-2
EC-like_1-1
CA-2
CA-1
EE-3
EE-2
EE-1
ISC/EB-5
ISC/EB-4
ISC/EB-3
ISC/EB-2
ISC/EB-1
Tk
Delta
Klu
E(spl)m3-HLH
Dh31
CCHa2
NPF
Pros
Gambicin
Tret1
CTL
trypsin-1
trypsin-7
nub
trypsin-5
CAH2
AQPcic
AQPan.G
Nha1
B
EC-like_1
EC-like_2
EC
CA
EE
ISC/EB
umap_2
umap_1
Percent Expressed
0
25
50
75
Average Expression
2
1
0
-1
CA
EC
EC-like_1
EC-like_2
EE
ISC/EB
C
Sugar
Blood
Infected
CA-1
CA-2
EC
EC-like_1-1
EC-like_1-2
EC-like_1-3
EC-like_1-4
EC-like_1-5
EC-like_2-1
EC-like_2-2
EC-like_2-3
EE-1
EE-2
EE-3
ISC/EB-1
ISC/EB-2
ISC/EB-3
ISC/EB-4
ISC/EB-5
D
Tk
E
Delta
F
Nha1
G
CTL
H
Pros
I
Gambicin
J
nub
K
trypsin-7
Expression Level


Cardia
EC
EC-like_1
EC-like_2
EE
ISC/EB
Percent Expressed
0
25
50
75
100
32608 AQPcic
41502 cp-like
42351 trypsin-5
37199 SNAT1-like
35847 lipase-H
34725 nub
34155 trypsin-7
41338 trypsin-1
39435 CTL
39362 Tret1
32045 Gambicin
32590 Orco
36596 CCHa2
32396 Dh31
34229 Tachykinin
40636 NPF
44963 Pros
41957 Klu
36824 Delta
33599 Tk
ISC/EB-1_Sugar
ISC/EB-1_Blood
ISC/EB-1_Infected
ISC/EB-2_Sugar
ISC/EB-2_Blood
ISC/EB-2_Infected
ISC/EB-3_Sugar
ISC/EB-3_Blood
ISC/EB-3_Infected
ISC/EB-4_Sugar
ISC/EB-4_Blood
ISC/EB-4_Infected
ISC/EB-5_Sugar
ISC/EB-5_Blood
ISC/EB-5_Infected
EE-1_Sugar
EE-1_Blood
EE-1_Infected
EE-2_Sugar
EE-2_Blood
EE-2_Infected
EE-3_Sugar
EE-3_Blood
EE-3_Infected
CA-1_Sugar
CA-1_Blood
CA-1_Infected
CA-2_Sugar
CA-2_Blood
CA-2_Infected
EC-like_1-1_Sugar
EC-like_1-1_Blood
EC-like_1-1_Infected
EC-like_1-2_Sugar
EC-like_1-2_Blood
EC-like_1-2_Infected
EC-like_1-3_Sugar
EC-like_1-3_Blood
EC-like_1-3_Infected
EC-like_1-4_Sugar
EC-like_1-4_Blood
EC-like_1-4_Infected
EC-like_1-5_Sugar
EC-like_1-5_Blood
EC-like_1-5_Infected
EC_Sugar
EC_Blood
EC_Infected
EC-like_2-1_Sugar
EC-like_2-1_Blood
EC-like_2-1_Infected
EC-like_2-2_Sugar
EC-like_2-2_Blood
EC-like_2-2_Infected
EC-like_2-3_Sugar
EC-like_2-3_Blood
EC-like_2-3_Infected


A
lipid catabolic process
protein deubiquitination
steroid metabolic process
protein modification by small protein removal
hormone metabolic process
antibiotic catabolic process
terpenoid metabolic process
post-translational protein modification
small molecule catabolic process
monocarboxylic acid metabolic process
steroid binding
organic acid transmembrane transporter activity
carboxylic acid transmembrane transporter activity
amino acid transmembrane transporter activity
organic anion transmembrane transporter activity
peptidase activity
carbon-carbon lyase activity
monocarboxylic acid binding
monoatomic anion transmembrane transporter activity
aminopeptidase activity
proteasome complex
endopeptidase complex
peptidase complex
proteasome core complex
proteasome core complex, alpha-subunit complex
peroxisomal matrix
microbody lumen
vesicle lumen
proteasome regulatory particle, base subcomplex
cytosolic proteasome complex
GO Term Description
0
5
10
15
-log10(q value)
Biological process
Molecular function
Cellular component
B
15
10
5
0
-5
avg_log2FC
44825 lipase
36152 MCM7
34108 FAH2
34096 CHYMO
32850 MCM4
31384 aladin
43938 FAH2
33374 FAAH2
-0.5
0.0
0.5
1.0
Difference of percentage of cells
Down
NS
Up
C
Average transcription count
ASTEI20_033917
ASTEI20_032608
ASTEI20_039638
ASTEI20_045421
Genes in EC-like_1 and EC-like_2
D
Average transcription count
ASTEI20_035338
ASTEI20_039804
ASTEI20_031615
Niemann-Pick Type C2 genes in EEs


A
17
17
7
2
0
0
15
10
5
0
Number of infected cells
ISC/EB
EE
EC-like_1
CA
EC
EC-like_2
Cell type
B
0.63
0.69
0.53
0.21
0
0
0.6
0.4
0.2
0.0
Percentage of infected cells (%)
ISC/EB
EE
EC-like_1
CA
EC
EC-like_2
Cell type


A
esg
Hsp70A1-like
Hsp70A1
ADA2
Dh-like
Hsp83-like
Hsp83
avg_log2FC
Difference of cell ratio
Down
NS
Up
B
KEGG pathway description
Ether lipid metabolism
beta-Alanine metabolism
Fatty acid degradation
Other glycan degradation
Pentose and glucuronate interconversions
Arginine and proline metabolism
Sphingolipid metabolism
Porphyrin metabolism
Glutathione metabolism
Steroid hormone biosynthesis
Ascorbate and aldarate metabolism
Retinol metabolism
Drug metabolism - cytochrome P450
Drug metabolism - other enzymes
Metabolism of xenobiotics by cytochrome P450
-log10(pValue)
C
KEGG pathway description
Metabolism of xenobiotics by cytochrome P450
Sphingolipid metabolism
Glycerolipid metabolism
Retinol metabolism
Galactose metabolism
Drug metabolism - other enzymes
Pentose and glucuronate interconversions
Ether lipid metabolism
Porphyrin metabolism
Insect hormone biosynthesis
Inositol phosphate metabolism
Starch and sucrose metabolism
Lipoic acid metabolism
Purine metabolism
Caffeine metabolism
-log10(pValue)
Xenobiotics biodegradation and metabolism
Metabolism of cofactors and vitamins
Carbohydrate metabolism
Lipid metabolism
Metabolism of other amino acids
Amino acid metabolism
biosynthesis and metabolism
Biosynthesis of other secondary metabolites
Nucleotide metabolism
Metabolism of terpenoids and polyketides


ISC/EB
EE
CA
EC
EC-like_1
ISC/EB
EE
CA
EC
EC-like_1
20
15
10
5
0
36974 Spn28Dc
45150 CLIPC3
30906 CLIP5B
38438 CLIPB16
35300 SCRAC1
42413 SCRB7
41298 GALE3
35199 galectin-4
31453 galectin-9
46038 AGO2
31961
43100
31687
40616 Drosha
31830
39435
32045
38293 Def
35066 cecropin-B
42620 cecropin-A
34602 Stat92E
36821 Dome
41097
37039
46157 PGRP-LB
38075 PGRP-LF
44130
35004
44168
43767 akirin
35343
40912
38162
35373 Cactus
38199
44951 Dorsal
42143
CLIP
SCR
GALE
SRRP
CTL
LRIM
RNAi
LYS
AMP
JAK-STAT
PGRP
IMD
TOLL
Blood-fed
Infected blood-fed